Journal of Theoretical Biology 437 (2018) 261–285

Contents lists available at ScienceDirect

Journal of Theoretical Biology

journal homepage: www.elsevier.com/locate/jtbi

Reentrainment of the circadian pacemaker during jet lag: East-west asymmetry and the effects of north-south travel

Casey O. Diekman[a,b,*], Amitabha Bose[a,b]

[a] Department of Mathematical Sciences, New Jersey Institute of Technology, Newark, NJ 07102 USA
[b] Institute for Brain and Neuroscience Research, New Jersey Institute of Technology, Newark, NJ 07102 USA

ARTICLE INFO

Article history:
Received 12 May 2017
Revised 7 September 2017
Accepted 3 October 2017
Available online 4 October 2017

Keywords:
Biological rhythms
Entrainment
Circadian oscillator
Light-dark cycles
Poincaré map
Translatitudinal travel

ABSTRACT

The normal alignment of circadian rhythms with the 24-h light-dark cycle is disrupted after rapid travel between home and destination time zones, leading to sleep problems, indigestion, and other symptoms collectively known as jet lag. Using mathematical and computational analysis, we study the process of reentrainment to the light-dark cycle of the destination time zone in a model of the human circadian pacemaker. We calculate the reentrainment time for travel between any two points on the globe at any time of the day and year. We construct one-dimensional entrainment maps to explain several properties of jet lag, such as why most people experience worse jet lag after traveling east than west. We show that this east-west asymmetry depends on the endogenous period of the traveler's circadian clock as well as daylength. Thus the critical factor is not simply whether the endogenous period is greater than or less than 24 h as is commonly assumed. We show that the unstable fixed point of an entrainment map determines whether a traveler reentrains through phase advances or phase delays, providing an understanding of the threshold that separates orthodromic and antidromic modes of reentrainment. Contrary to the conventional wisdom that jet lag only occurs after east-west travel across multiple time zones, we predict that the change in daylength encountered during north-south travel can cause jet lag even when no time zones are crossed. Our techniques could be used to provide advice to travelers on how to minimize jet lag on trips involving multiple destinations and a combination of transmeridian and translatitudinal travel.

1. Introduction

Circadian clocks have evolved to align biological functions with the 24-h environmental cycles conferred by the rotation of the earth (Johnson et al., 2003). In humans, a central circadian pacemaker coordinates various physiological rhythms so that they peak at the appropriate time of the day, such as the release of the sleep-promoting hormone melatonin in the evening and the wake-promoting hormone cortisol in the morning (James et al., 2007). The endogenous period of the human circadian oscillator in the absence of external time cues is not exactly 24 h (Czeisler et al., 1999). The period of the oscillator becomes 24 h under normal circumstances when exposed to natural environmental cycles, and a stable phase relationship between the oscillator and its environment is established: the oscillator is phase-locked or *entrained* to the external cycles (Wright et al., 2013). For circadian oscillators, the strongest entraining signal is the daily light-dark (LD) cycle (Duffy and Wright, 2005). If entrainment is disrupted by a sudden shift in the phase of the LD cycle, for example due to rapid travel across time zones, then the phase of the circadian oscillator undergoes adjustments until phase-locking is reestablished and the oscillator is reentrained (Aschoff et al., 1975).

Jet lag is a collection of symptoms experienced after rapid transmeridian travel. These symptoms—such as insomnia, excessive daytime sleepiness, gastrointestinal disturbances, and general malaise—are not simply due to travel fatigue following a long flight, but rather are caused by misalignment of the traveler's internal circadian clock with the environmental cycles in the new time zone (Sack, 2009). Each year about 30 million US residents fly to overseas destinations (U.S. Citizen Travel to International Regions, 2017). For international business travelers, athletes, or government and military personnel, jet lag can impair judgment, hinder performance, or threaten public safety (Eastman and Burgess, 2009). Most travelers experience more severe jet lag after flying east than after flying west (Waterhouse et al., 2007), and a recent analysis of

* Corresponding author.
E-mail address: diekman@njit.edu (C.O. Diekman).

https://doi.org/10.1016/j.jtbi.2017.10.002
0022-5193/

over 20 years of data from Major League Baseball games found that jet lag impairs performance moreso after eastward than westward travel (Song et al., 2017). The conventional explanation for this directional asymmetry in jet lag severity is that since the human circadian clock typically has an endogenous period of greater than 24 h, it is easier to phase delay the clock in response to the phase delay of the LD cycle caused by westward travel than it is to phase advance the clock in response to the phase advance of the LD cycle caused by eastward (Eastman and Burgess, 2009). Reentraiment though phase adjustment in the same direction as the shift of the LD cycle is referred to as *orthodromic*. After long trips, some travelers reentrain *antidromically* or through phase adjustments in the opposite direction of the phase shift of the LD cycle, i.e. phase delays after traveling east and phase advances after traveling west (Arendt et al., 1987; Klein and Wegmann, 1977; Takahashi et al., 2001).

In this paper we use a mathematical model of the human circadian pacemaker, the Forger–Jewett–Kronauer (FJK) model (Forger et al., 1999), to explain the existence of east-west asymmetry in jet lag severity and the antidromic mode of reentrainment. The FJK model is a widely accepted model in the circadian literature that captures both phase and amplitude dynamics of daily core body temperature oscillations. It has been fit to experimental data on how light affects human circadian rhythms and has been used in several studies to design schedules that minimize jet lag (Dean et al., 2009; Serkh and Forger, 2014; Zhang et al., 2016). Consistent with a recent study employing a phase-only model (Lu et al., 2016), we find that the endogenous period of the circadian oscillator does influence east-west asymmetry. Differently than (Lu et al., 2016), however, we find that the period being greater than or less than 24 h is not the critical factor. Furthermore we show that daylength, and therefore the season of the year, affects whether eastward or westward travel is worse.

The medical definition of jet lag requires travel across time zones, implying that strictly north-south or translatitudinal travel within the same time zone cannot cause jet lag. We take a broader view of jet lag as symptoms resulting from any travel-induced misalignment of the circadian clock and the external LD cycle, and argue that the change in daylength experienced when traveling across latitudes (for example between the northern and southern hemispheres) in the summer or winter may disrupt entrainment. The question of whether purely north-south travel can result in significant misalignment has received very little attention in the literature. We find that in the FJK model, a difference in the daylength between departure and destination cities is enough to cause jet lag on the order of several days (depending on parameters) even with no change in time zone. Combining our findings on east-west travel with those on north-south travel, we also investigate travel that incorporates both of these directions. By considering a hypothetical case study involving travel between four cities located in North America, South America, Asia, and Australia, we show that the north-south component of travel can significantly add to or reduce reentrainment times even in cases where strict north-south travel itself incurs no jet lag.

The main tool we use to gain insights into the properties of jet lag is the *entrainment map*, a technique we recently introduced for calculating the LD-entrained solution of an oscillator subjected to external periodic forcing consisting of N hours of light and $24-N$ h of darkness (Diekman and Bose, 2016). The method involved deriving a one-dimensional map, $\Pi(x)$, whose fixed points corresponded to stable or unstable entrained periodic solutions. We showed that the entrainment map yields more accurate predictions about the phase of the stable entrained solution than methods based on phase response curves. In Diekman and Bose (2016), we showed how the entrainment map for the two-dimensional Novak-Tyson model of the *Drosophila* molecular clock (Tyson et al., 1999) depends on parameters of the model and how it can be used to determine regimes over which solutions entrain through phase advance or phase delay. The entrainment map was then applied to higher dimensional systems such as the three-dimensional Gonze et al. (2005) and the 180-dimensional Kim and Forger (2012) models of the mammalian molecular clock.

Here we build entrainment maps for the FJK model to explore various facets of reentrainment after travel. Travel can involve a change of time zone, such as eastward or westward travel, a change in photoperiod, such as northward or southward travel, or a combination of both, such as travel from North America to Australia. We show that reentrainment properties depend both quantitatively and qualitatively on key parameters including the endogenous period of the oscillator, the daylength, and the intensity of light. Using our methods, we can calculate reentrainment times for travel between any two locations on the globe, at any time of the year, and for any departure or arrival time. In doing so, we are able to explain that the east-west asymmetry of jet lag is a generic feature of the FJK model that is highly dependent on both the endogenous period of the traveler as well as the daylength. Using a generalization of the concept of neutral period introduced by Aschoff et al. (1975), we show that for different combinations of these two parameters, travel to the east can incur more jet lag than travel to the west or vice versa. In fact, because of seasonal changes in the daylength, for the same traveler a journey in one direction may be harder in the winter, while a journey in the opposite direction may be harder in the summer. Our findings are related, in part, to those of Herzel and collaborators (Bordyugov et al., 2015; Granada and Herzel, 2009; Schmal et al., 2015) who have characterized the phase of entrainment as a function of endogenous period, zeitgeber (external stimulus) strength, and photoperiod for several different circadian models using Arnold tongues and Arnold onions. The analysis of the entrainment map also provides insight into the different modes of reentrainment. Prior work using a model of the mammalian molecular clock identified a threshold separating orthodromic and antidromic modes of reentrainment, but did not explain what mathematical object might act as the threshold (Leloup and Goldbeter, 2013). Here we show that the unstable fixed point of the entrainment map can be used to predict the threshold that separates the two modes of reentrainment.

Contrary to what one might naively expect, we find that reentrainment time is relatively independent of departure or arrival time, and that the longest trips do not necessarily give rise to the longest reentrainment times. Instead, the worst-case trip is determined by the ordering and magnitude of the distance between the stable and unstable fixed points of the entrainment map, which themselves are dependent on the internal body clock and daylength. We find that for low light intensities, trips that place the traveler in a neighborhood of the unstable fixed point of the map will give rise to the longest reentrainment times. For higher light intensities, the longest reentrainment times still occur in a neighborhood of the unstable fixed point, but there is also the potential for dramatically short reentrainment times for certain trips within this neighborhood. These dramatically short reentrainment times are associated with amplitude suppression and a phase singularity, and have been observed previously in the FJK model at high light intensity (Serkh and Forger, 2014).

In this study, we consider the light level to be fixed at either low or high intensity (lux) across the entire photoperiod. Admittedly, this is not a light protocol that a traveler is likely to experience. However, the main purpose of our study is to provide a mathematical explanation for why certain features of jet lag arise, such as east-west asymmetry and different modes of reentrainment. This is most easily explained using single lux levels. As further discussed throughout the paper, we expect the mechanisms

that underlie our findings to continue to exist under more realistic light schedules.

2. Model and methods

2.1. The Forger, Jewett, and Kronauer (FJK) model

The FJK model (Forger et al., 1999) for the human circadian rhythm utilizes a Van der Pol type oscillator and is based on prior models of Kronauer and collaborators (Jewett and Kronauer, 1998; Kronauer, 1990). It is a three-dimensional model given by

$$\frac{dC}{dt} = \frac{\pi}{12}(A+B) \tag{1}$$

$$\frac{dA}{dt} = \frac{\pi}{12}\left(\mu\left(A - \frac{4}{3}A^3\right) - C\left[\left(\frac{24}{0.99669\,\tau_c}\right)^2 + kB\right]\right) \tag{2}$$

$$\frac{dn}{dt} = \gamma\left(\alpha[I]f(t)\,(1-n) - \beta n\right) \tag{3}$$

$$B = G\alpha[I]f(t)(1-n)(1-0.4C)(1-0.4A) \tag{4}$$

$$\alpha[I] = \alpha_0\left[\frac{I}{I_0}\right]^p. \tag{5}$$

The variable C represents core body temperature, A is a phenomenological auxiliary variable, and n models the phototransduction pathway through which light drives the circadian system. The variable B captures circadian modulation of the oscillator's sensitivity to light. All parameter values are positive. In particular, τ_c determines the period of the oscillator in constant darkness, I codes for the intensity of light, and μ is a stiffness parameter that is related to the rate of amplitude growth or decay after the oscillator is perturbed off of its limit cycle. We refer to $\mu = 0.23, k = 0.55, \gamma = 60, \beta = 0.0075, G = 33.75, \alpha_0 = 0.05, I_0 = 9500, p = 0.5$ with $I = 1000$ lux and $\tau_c = 24.2$ h as the canonical set of parameters.

The function $f(t)$ is the light stimulus. We are interested in three distinct situations: constant darkness (DD), in which we set $f(t) \equiv 0$; constant light (LL) in which $f(t) \equiv 1$; and a 24-h light/dark (LD) photoperiod in which the lights are on for N hours and off for $24 - N$ h. During the dark portion of the LD photoperiod $f(t) = 0$, while during the light portion $f(t) = 1$. In constant darkness, $dn/dt = -\beta n$, therefore $n \to 0$ and the parameter β controls the rate of decay. In constant light, $dn/dt = \gamma(\alpha(I)(1-n) - \beta n)$ such that $n \to \alpha(I)/(\alpha(I) + \beta)$ with rate α_0. Note that α_0 is an order of magnitude larger than β which implies that n approaches its maximum when the lights turn on faster than it approaches its minimum when the lights turn off.

The A and C-nullclines are given by

$$\mathcal{N}_A: \quad C = \frac{\mu\left(A - \frac{4}{3}A^3\right)}{\left(\frac{24}{0.99669\,\tau_c}\right)^2 + kB} \tag{6}$$

$$\mathcal{N}_C: \quad A = -B. \tag{7}$$

The nullcline $\mathcal{N}_A$ is a cubic-shaped curve in the projection onto the $A - C$ space. During DD conditions, $B = 0$, and $\mathcal{N}_C$ is a vertical line that intersects $\mathcal{N}_A$ along its middle branch. This intersection corresponds to an unstable fixed point. Surrounding it is a stable periodic orbit, referred to as the DD limit cycle. The prefactors $\pi/12$ and 0.99669 that appear in (2), and the value of $\mu = 0.23$, were chosen such that the period of this limit cycle is very close to τ_c hours (Forger et al., 1999). The period of the DD limit cycle is referred to as the endogenous period. The value of the roots of $\mathcal{N}_A$ are $A = 0, \pm\sqrt{3}/2$ independent of τ_c. Increasing τ_c makes the A-nullcline have steeper left and right branches. This results in a decrease in the amplitude of dA/dt, thereby slowing down oscillations. As a result, the intrinsic period of the DD oscillator is an increasing function of τ_c. Under LL conditions, although n is constant, B depends on A and C. Using Eq. (4), and substituting into Eq. (7), yields a monotone increasing $\mathcal{N}_C$ nullcline that continues to intersect $\mathcal{N}_A$ along its middle branch. As a result, an LL limit cycle also exists. The period of the LL limit cycle is less than τ_c hours. The LL period is also an increasing function of τ_c, for the same reasons as the DD period. When the model is considered under LD conditions, depending on parameters, a periodic solution may exist. When the period of the solution matches that of the LD forcing (24 h), we call it an LD-entrained solution.

2.2. The entrainment map Π(x)

The entrainment map $\Pi(x)$ is a return map for initial conditions lying on a Poincaré section that return to it at a later time. A Poincaré section is a lower-dimensional slice (hyperplane) of the original phase space. Both in theory and in practice, we have freedom to choose the location of the section, provided that we know that a trajectory starting on it will return to it later in time. Because the FJK model uses a Van der Pol type oscillator, we have considerable knowledge of how trajectories evolve in phase space. For the sake of illustration, choose the Poincaré section, $\mathcal{P}$, at $A = 0$, with $A' < 0$, which yields a rectangle in the C and n space. Assume that an oscillator has an initial condition that lies on $\mathcal{P}$ with $n = 0$ and the C value chosen as the value at the intersection with the DD limit cycle. Let x denote the number of hours since the lights last turned on. Evolve the trajectory under the flow until it again returns to $\mathcal{P}$. Call this time $\rho(x)$. The entrainment map $\Pi(x)$ is defined as the amount of time that has passed since the most recent onset of the lights. In Diekman and Bose (2016), we showed that $\Pi(x) = (x + \rho(x)) \mod 24$, which yields a one-dimensional map. Because of the mod 24 operation, the map Π may have a discontinuity. The entrainment map has certain generic properties (Diekman and Bose, 2016): it maps the interval [0,24] onto itself, it has at most one point of discontinuity, it is increasing at each point of continuity, and it is periodic in that $\Pi(0^+) = \Pi(24^-)$. Moreover, it depends continuously on parameters of interest such as τ_c, N, and I.

A fixed point x^* of the entrainment map satisfies $\Pi(x^*) = x^*$. It corresponds to the situation where the trajectory has left $\mathcal{P}$ x^* hours after the lights turned on, and then returns to $\mathcal{P}$ exactly 24 h later when the lights have again most recently turned on x^* hours ago. The fixed point is stable if $|\Pi'(x^*)| < 1$ and unstable otherwise. We will show that over a wide range of parameters, there are typically two fixed points of the map, x_s which is stable, and x_u which is unstable. Whether the fixed points of the map correspond to actual stable and unstable periodic orbits of the system of Eqs. (1)–(3) is a delicate issue. A trajectory starting on the Poincaré section $\mathcal{P}$ at $A = 0$ would have unknowns C, n, and x. A three-dimensional return map would track the values of the unknowns and return new values of C, n, and x when the trajectory returns to $\mathcal{P}$. The entrainment map however only tracks whether x has returned to its original value, not whether C and n have. As described below, the stable fixed point x_s of the map corresponds to a stable periodic orbit in all the cases we considered. The existence of the unstable fixed point of the map x_u has different implications depending on the light intensity. At low light intensity, the unstable fixed point corresponds to an unstable periodic orbit in the full phase space. x_u also demarcates a region in phase space that separates trajectories that reentrain through either phase advance or phase delay. At larger light intensities, there does not appear to be an unstable

periodic orbit that corresponds to x_u. Nonetheless this fixed point still separates the direction of reentrainment. x_u is also related to trajectories that can reentrain unusually fast. In the Appendix, we further elaborate on the mathematical correspondence between x_s, x_u, and dynamics of the full system of equations.

To explore various forms of jet lag, we will use a set of entrainment maps that are constructed with Poincaré sections corresponding to every half-hour. These sections are chosen by obtaining the LD-entrained solution numerically, and then dividing up this LD-entrained solution into half-hour time intervals, starting with $X = 0$ corresponding to lights on at a nominal choice of 7 AM. Radial Poincaré sections emanating from the origin $(A = 0, C = 0)$ and passing through these half-hour marks are then constructed. The section is then extended to a rectangle by allowing n to vary between 0 and 1. We define $\Pi_X(x)$ to denote the map obtained by choosing the Poincaré section X hours from lights on. By construction of the map $\Pi_X(x)$, the stable fixed point x_s of the map occurs exactly at X, that is $x_s = X$, since 7 AM denotes both the time of lights on and $X = 0$. When we build an entrainment map using initial conditions that lie on the LD-entrained solution, then at a stable fixed point of the map all of the dependent variables C, n, and x return to their original values. In this case, the stable fixed point does correspond to a stable periodic solution.

We shall be interested in the transient time it takes a trajectory that has an initial condition that lies off of the LD-entrained solution to enter a neighborhood of it. Specifically, consider a Poincaré section taken along the LD-entrained solution X hours after the lights turn on. Take an initial condition that lies at the intersection of the LD-entrained solution and this Poincaré section, but with $x_0 \neq x_s$, x_u. In this case, the trajectory will not initially be entrained since the LD cycle will be offset by $|x_s - x_0|$ hours. This means that the first return time $\rho(x_0) \neq 24$. We will say that a trajectory is entrained if there exists a $k \geq 0$ such that $|\rho(x_j) - 24| < 0.5$ for $j \geq k$, where $x_j = \Pi(x_{j-1})$. Entrainment is said to occur on $(k+1)$th cycle. The total entrainment time is simply $\Sigma_{j=0}^{k} \rho(x_j)$. In terms of the map, $\Pi(x)$ entrainment is equivalent to $|\Pi(x_j) - x_s| < 0.5$.

3. Results

3.1. The LL, DD, and LD-entrained limit cycles of the FJK model

The DD limit cycle is obtained when $f(t) \equiv 0$. In this case, $B = 0$ and $dn/dt = -\beta n$, thus $n \to 0$. Since the DD limit cycle is restricted to $n = 0$, it can be found by solving the planar system given by Eqs. (1) and (2). Those equations are of standard Van der Pol oscillator type that possess a stable limit cycle. The A-nullcline is cubic, the C-nullcline is linear, and they intersect at an unstable fixed point on the middle branch. The DD trajectory encloses that unstable point. Similarly, the LL oscillator is obtained when $f(t) \equiv 1$. Now, $n \to \alpha[I]/(\alpha[I] + \beta)$ and B can be written in terms of A and C. So the model is again planar with a cubic nullcline and one that is monotone increasing. They intersect along the middle branch of the cubic, forming an unstable fixed point. For the canonical set of parameters (defined in Section 2.1), the period of the DD oscillator is τ_c, whereas the period of the *LL* oscillator (23.96 h) is less than τ_c.

In Fig. 1, we plot the DD, LL, and LD-entrained oscillations for $N = 12$ h, $I = 1000$ lux. Panel A shows the time traces of each of these oscillations, Panel B shows them in the 3-dimensional $A - C - n$ phase space, and Panel C shows them projected onto the $A - C$ phase plane. Note that the LD-entrained oscillation tracks towards the DD oscillation during darkness and towards the LL oscillation during light. The transition of the trajectory from DD to LL is fairly rapid, while that from LL to DD is relatively slow since β is small compared to α_0. Hourly markings (open red or black circles) are placed on the LD-entrained cycle where lights on corresponds to 7 AM and lights off to 7 PM.

In Fig. 2A and B, we plot $\rho(x)$ and $\Pi(x)$ for the canonical set of parameters using the $A = 0, A' < 0$ Poincaré section. The graph of $\rho(x)$ intersects the horizontal line corresponding to 24 h at two points, x_s and x_u. These points represent return times of exactly 24 h. Also note that because of periodicity $\rho(0^+) = \rho(24^-)$. The graph of $\Pi(x)$ intersects the diagonal at the fixed points x_s and x_u. The slope at the points of intersection determines the stability of these fixed points.

In Fig. 2C and D, we show two examples of reentrainment, both in the map and in simulations. The green trajectory in Panel C shows the cobweb diagram for a trajectory that starts with an initial condition that is less than x_u. The cobwebbed trajectory moves to the left with each iterate indicating a phase advancement. The corresponding green time trace in Panel D confirms this in its approach to the LD-entrained solution (solid black trace). The magenta trajectory in Panel C shows a trajectory that starts with an initial condition to the right of x_u, and entrains though phase delays as the iterates of the cobweb move to the right, over the discontinuity, before approaching x_s. The magenta trace in Panel D shows how the oscillator phase delays at each cycle until entrainment. Thus the unstable fixed point of the map x_u separates initial conditions of trajectories that entrain in direct simulations through phase advance or phase delay. What is particularly interesting about this agreement is the fact that we have found no evidence that an unstable periodic orbit actually exists for $I = 1000$ lux. Instead, the stable periodic orbit seems to be globally attracting. Locally near x_s and the stable periodic orbit, trajectories approach the fixed point by either advancing or delaying. Therefore there must be a structure elsewhere in phase space that separates trajectories that become phase advancing or phase delaying. We speculate that the unstable fixed point x_u of the map indicates where in phase space to look for such a structure. We provide further evidence for this conjecture in the Appendix; however, fully characterizing this structure mathematically is beyond the scope of this paper.

3.2. The dependence of Π(x) on parameters

The entrainment map $\Pi(x)$ depends continuously on parameters. In particular, we are interested in how the map changes with variations in τ_c, N, and I. The dependence on parameters is qualitatively the same as what we found in our earlier study (Diekman and Bose, 2016) of the Novak-Tyson model of the molecular circadian clock in *Drosophila* (Novak and Tyson, 2008), and is consistent with general theories on the phase of circadian entrainment (Bordyugov et al., 2015). To understand this dependence, we vary one parameter at a time with the others set at their canonical values.

Consider first changes in the intrinsic period τ_c. Fig. 3A and B show how the maps $\rho(x)$ and $\Pi(x)$ depend on τ_c. The return time map $\rho(x)$ is a monotone function of the parameter τ_c. This has to do with how the A nullcline, $\mathcal{N}_A$, changes with τ_c. As discussed in Section 2.1, for both the DD and LL cases, the steepness of the right and left branches of the cubic increases with τ_c, leading to increases in the period of each of these oscillators (Fig. 3C and D). To illustrate this, consider the two extreme cases $\tau_c = 22.2$ h and 27.2 h with an initial condition of $x_0 = 18$. Fig. 3C shows the ensuing trajectories leaving the Poincaré section $A = 0$ projected onto the $A - C$ plane. Since $x_0 = 18$, the trajectories are initially subjected to six hours of darkness and thus they follow the corresponding DD dynamics. After six hours of evolution, the green trajectory ($\tau_c = 22.2$ h) is about an hour ahead of its magenta counterpart ($\tau_c = 27.2$ h). The green trajectory moves faster horizontally since its nullcline is further away. For the next 12 h, the trajectories evolve

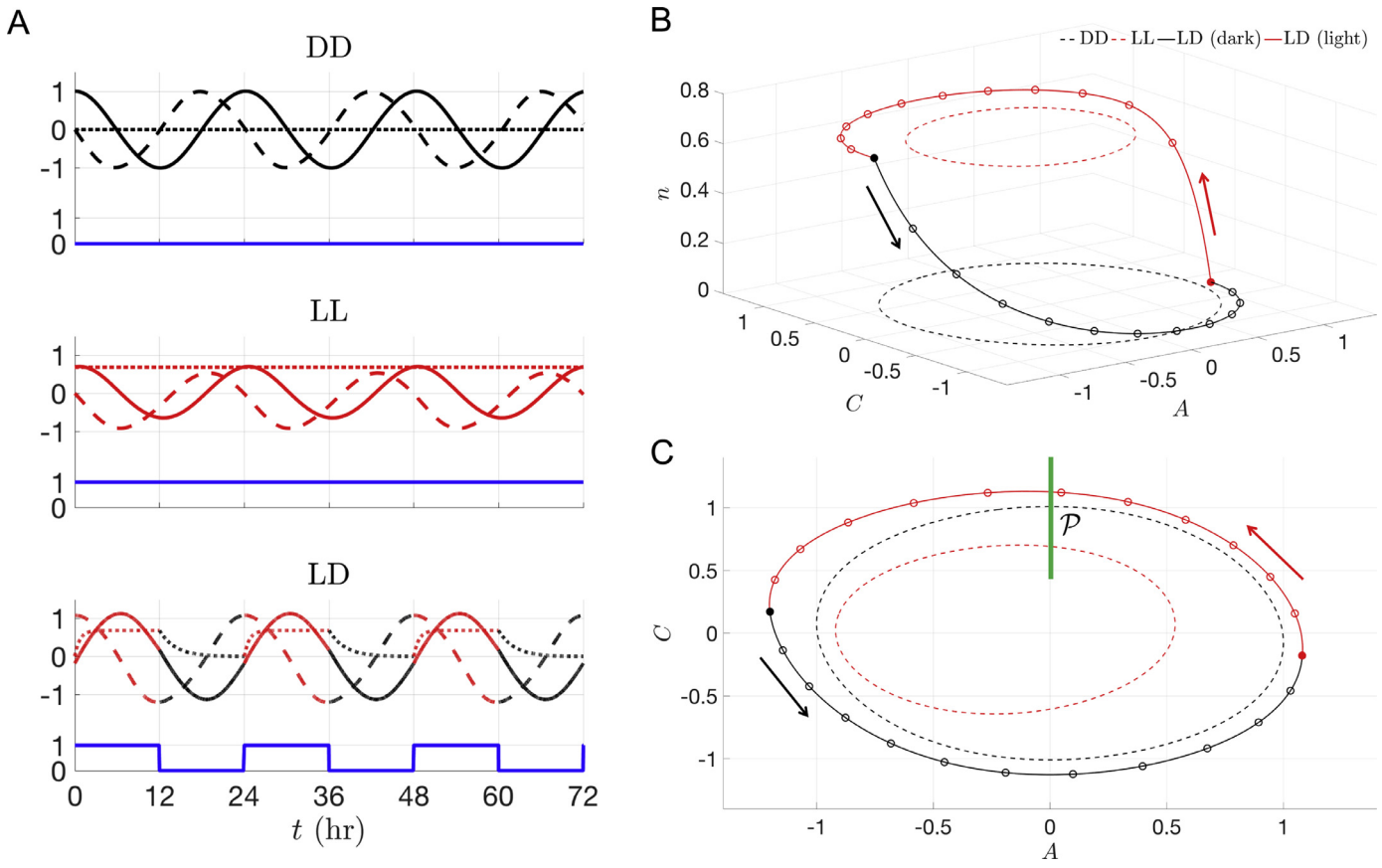

Fig. 1. FJK model DD, LL, and LD limit cycles for $\tau_c = 24.2$ h, $N = 12$ h, $I = 1000$ lux. (A) Time course of model variables in constant darkness (top), constant light (middle), and a 12:12 light-dark cycle (bottom). The variable C is shown as solid lines (black in DD, red in LL, and red/black in LD), the variable A as dashed lines, and the variable n as dotted lines. The light stimulus function $f(t)$ is shown as solid blue lines. The DD, LL, and LD limit cycles in the 3-dimensional $A-C-n$ phase space (B) and projected onto the 2-dimensional $A-C$ phase plane (C). A 1-dimensional projection of the Poincaré section $\mathcal{P}$ at $A = 0$ ($A' < 0$) is shown in green. (For interpretation of the references to color in this figure legend, the reader is referred to the web version of this article.)

under conditions of light, as shown in Fig. 3D. The $\tau_c = 22.2$ h trajectory moves further ahead of the other, now by about three hours. Again the green trajectory moves faster horizontally. Finally, for the last portion of their evolutions back to the Poincaré section, they evolve under darkness; Fig. 3C. In general, the dynamics of the LD-forced oscillator are determined by the LL limit cycle when the lights are on and by the DD limit cycle when the lights are off. Thus, independent of whether the LD-forced oscillator is in a current situation of lights on or off, its dynamics will always be slower when τ_c is greater. Therefore $\rho(x)$ will be larger for larger τ_c.

In Fig. 3B we show how $\Pi(x)$ depends on τ_c. Increasing τ_c causes the maps to shift up. This is a consequence of $\rho(x)$ being a monotone increasing function of τ_c. This causes the stable fixed point x_s to increase (and the unstable fixed point x_u to decrease). This means that individuals with slower intrinsic body clocks reach their maximum or minimum core body temperatures later in the day. The opposite is true when τ_c is decreased below 24.2 for individuals with faster than normal intrinsic body clocks. The maps shift down and the stable fixed point x_s decreases (and x_u increases). Note that as τ_c increases, the distance between x_s and x_u decreases. When τ_c becomes large enough, these two fixed points merge at a saddle-node bifurcation, implying the loss of entrainment and providing an upper bound on the range of entrainment. Similarly, when τ_c decreases and becomes too small, a different saddle-node bifurcation of these two fixed points occurs signifying the lower bound on the range of entrainment.

In Fig. 4A and B, we show how the entrainment map varies with changes in light intensity I (Panel A) and photoperiod (Panel B). Changing light intensity I has a pronounced effect on the shape of the maps, but less of an effect on the location of the stable and unstable fixed points (Fig. 4A). The increased concavity with stronger intensity light leads, in general, to faster entrainment (discussed in greater detail in Diekman and Bose, 2016). The map becomes insensitive to increases in I above a certain point, with nearly complete overlap of the maps for $I = 100,000$ lux and above. This suggests that entrainment cannot be lost by increasing the light intensity too much. On the other hand, if the light intensity becomes too weak ($I \to 0$), then entrainment is lost through a saddle-node bifurcation as the maps move up and the stable and unstable fixed points collide. Changes to the photoperiod, $N : 24 - N$, are shown in Fig. 4B. An increase in N, meaning longer daylength, shifts the discontinuity of the map to the right because the portion of the map to the right of x_s gets shifted down. To the left of x_s, the opposite happens where an increase in N shifts the map up. Note that the distance between x_s and x_u decreases with N. This change in distance is a critical factor in explaining the east-west asymmetry of jet lag, as discussed in Section 3.4.

Information from entrainment maps can be used to construct plots that display the entrainment region as a function of two parameters, known as *Arnold tongues* or *Arnold onions*. In Fig. 4C and D, we show the stable phase of entrainment for different parameter pairs. The stable phase was determined by constructing an entrainment map at each set of parameter values, and then find-

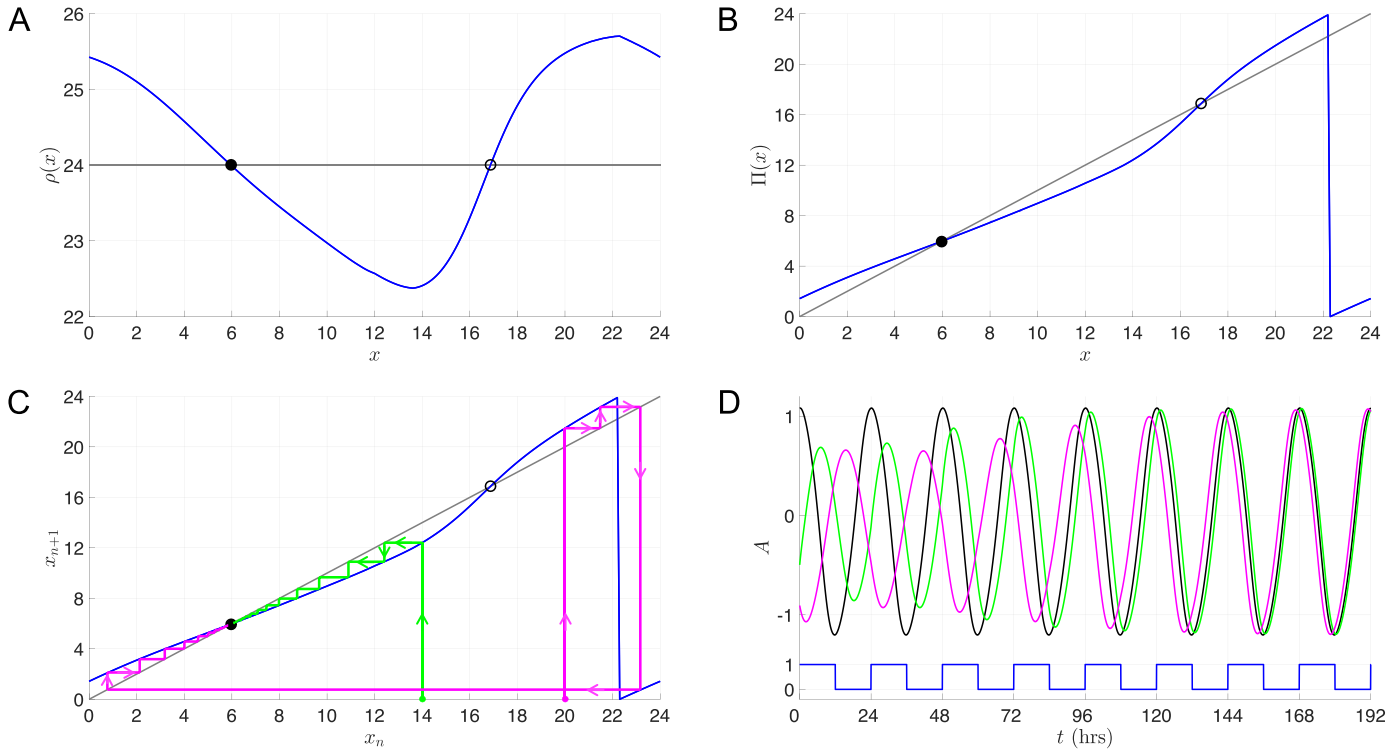

Fig. 2. Entrainment map and reentrainment simulations. Parameters: $\tau_c = 24.2$ h, $N = 12$ h, and $I = 1000$ lux. (A) $\rho(x) = 24$ at $x = 5.96$ (solid dot) and $x = 16.87$ (open dot). (B) These x values satisfy $\Pi(x) = x$ and correspond to stable and unstable fixed points, x_s and x_u, of the entrainment map. (C) Cobwebbing the entrainment map shows that x_u separates initial conditions that reentrain through phase advance (green) and phase delay (magenta). (D) Direct simulations for initial conditions lying on opposite sides of x_u showing reentrainment through phase advances (green) and phase delays (magenta) as predicted by the entrainment map. (For interpretation of the references to color in this figure legend, the reader is referred to the web version of this article.)

ing the location of the stable fixed point x_s. The Arnold tongue in Fig. 4C displays the entrainment region and stable entrained phase as a function of endogenous period τ_c and light intensity I for $N = 12$ h. The colored region of parameter space represents parameter pairs for which stable entrainment occurs, and curves of constant phase lie on curves of constant color. For illustrative purposes, the curve with $x_s = 6$ is shown in white. As I increases, curves of constant phase become almost vertical indicating that increasing light intensity does not significantly change the phase of entrainment (as noted in Fig. 4A). Horizontal slices of Fig. 4C show that the range of endogenous periods that lead to entrainment increases with intensity. These results are consistent with those of Bordyugov et al. (2015), who calculated Arnold tongues for a Kuramoto model as well as a variety of circadian models including the Gonze et al. (2005) and Relógio et al. (2011) models. The Arnold tongues for those models formed a V-shaped region in parameter space, similar to the parabola-shaped region that we find here for the FJK model. Our results are also consistent with the laboratory study of Wright et al. (2001), which found that humans could entrain to very low intensity light (1.5 lux) if the forcing period was exactly 24 h, but could not entrain if the forcing period was different than 24 h (specifically 23.5 or 24.6 h). The Arnold onion in Fig. 4D displays the entrainment region and stable entrained phase as a function of τ_c and N for $I = 1000$ lux. The curve with $x_s = 6$ is again shown in white. For a fixed endogenous period (vertical slice of figure), changes in the photoperiod can have large and counterintuitive effects on the stable phase. For example, with $\tau_c = 24.5$ h and $N = 8$ h, the stable phase $x_s < 6$. If N is either increased enough, or decreased enough, the stable phase becomes $x_s = 6$. Thus changes in entrained phase are not necessarily monotonic with respect to changes in photoperiod. This figure is qualitatively similar to Fig. 1B of Schmal et al. (2015) who calculate Arnold onions for a host of models. The bottom tip of our onion is located at $\tau_c = 24$ h, corresponding to an endogenous period in constant darkness ($N = 0$) that is equal to the period of LD forcing that we used for $0 < N < 24$. The top tip of our onion is located at $\tau_c = 24.4$ h, which is close to the endogenous period in constant darkness that exhibits a 24-h period when placed in constant light ($N = 24$). The tilt of the onion to the right indicates that the FJK model is consistent with *Aschoff's Rule*, which states that $\tau_{LL} < \tau_{DD}$ for day-active animals. The Arnold onions in Schmal et al. (2015) are found by holding the endogenous period in constant darkness fixed at 24 h and varying the LD forcing period, whereas we vary the endogenous period in constant darkness and hold the LD forcing period fixed at 24 h. Thus their onions tilt to the left, rather than the right, for day-active animals.

3.3. Jet lag due to east-west travel

We now determine how long a traveler takes to reentrain after a change in time zone by computing, via direct simulation, reentrainment times for trips with a prescribed arrival time over a prescribed number of time zones (either east or west). We then use the entrainment map to explain the simulation results, as well as to explain the east-west asymmetry in jet lag.

Fig. 5 shows a schematic diagram of the 12:12 LD cycle across all time zones. The horizontal direction demarcates hourly intervals starting with 7 AM (defined as $X = 0$); the vertical direction demarcates hourly intervals corresponding to different time zones. The middle row of the diagram corresponds to the "home" time zone ($Z = 0$) while those lying above this row ($Z > 0$) correspond to travel to the east, and those below ($Z < 0$) correspond to travel to the west. In each row, the corresponding 12:12 LD cycle is shown such that lights turn on at 7 AM in the "destination" time zone. Each column shows the current position of the LD cycle in that

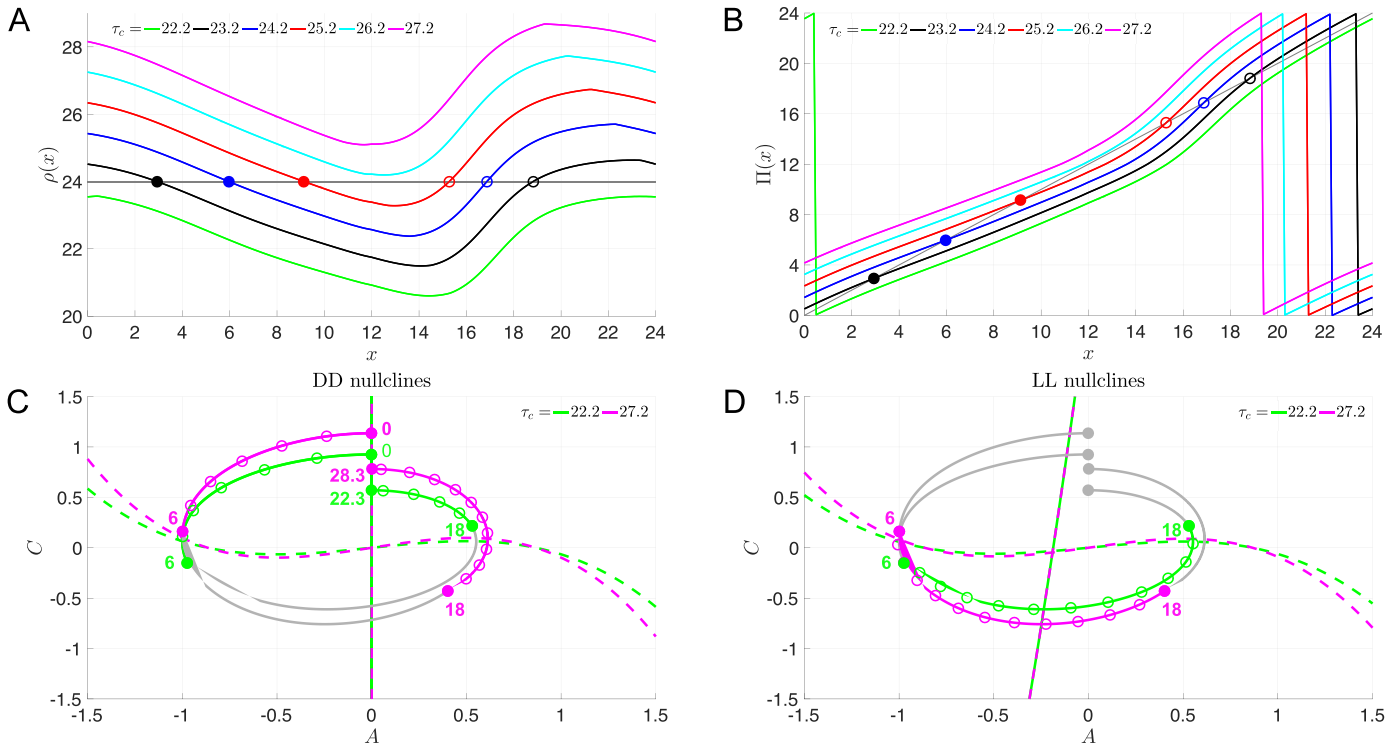

Fig. 3. Dependence of entrainment map on endogenous period τ_c. (A) $\rho(x)$ shifts up as τ_c increases and down as τ_c decreases. (B) $\Pi(x)$ shifts up and to the left as τ_c increases, causing the stable fixed point x_s (solid dots) to move to the right, implying that as intrinsic period increases the phase of entrainment becomes more delayed. The unstable fixed point x_u (open dots) move to the left. As τ_c decreases, $\Pi(x)$ and the fixed points move in the opposite manner. (C) and (D) Evolution of trajectories used in computation of $\rho(18)$. In (C), during the initial six hours of darkness the DD nullclines (dashed lines) are such that the $\tau_c = 27.2$ h oscillator moves slower than the $\tau_c = 22.2$ h oscillator; the green trajectory is ahead of the magenta. In Panel D, for the next 12 h of light, the LL nullclines (dashed lines) are such that the $\tau_c = 27.2$ h oscillator still moves slower than the $\tau_c = 22.2$ h oscillator when the lights are on. The final portions of their respective evolutions under darkness are shown in Panel C. Gray curves in each panel are copies of the colored curves in the opposite panels. In sum, the magenta trajectory moves slower than the green contributing to a larger $\rho(18)$ value and upward shift of the ρ map. For this figure $N = 12$ h and $I = 1000$ lux. (For interpretation of the references to color in this figure legend, the reader is referred to the web version of this article.)

zone. There are two natural ways to use this travel grid. One possibility is to assume that from departure, the traveler immediately tries to reentrain to the destination time zone (DTZ). The other is to assume that the traveler remains phase-locked to the home time zone (HTZ) throughout the duration of the trip and only begins to reentrain upon arrival at their destination. The former case is equivalent to studying the dynamics of a leaving time map, and the latter, the dynamics of an arrival time map. Both cases can be thought of as instantaneous travel time in that the traveler instantaneously switches from the HTZ to the DTZ. In what follows, let us take the latter interpretation of an arrival time map. Namely, we define the arrival time as the HTZ time when the destination is reached. For example, if one travels from New York to Los Angeles and arrives at 1 PM, this means they have arrived at 1 PM New York time (which corresponds to 10 AM Los Angeles time.)

In both the home and destination time zones, the 24-h LD forcing is identical, but phase shifted by Z hours. We construct a set of Poincaré maps associated with each arrival time X, denoted by $\Pi_X(x)$. An oscillator that is entrained in the home time zone to a value $x_s = \Pi_X(x_s)$ will also entrain to the same value x_s in the destination time zone if the Poincaré section is chosen at the same time location X along the LD-entrained cycle. In other words, the phase of entrainment to the LD cycle is the same, independent of the zone. Suppose the oscillator starts in its home time zone $Z = 0$ entrained to the 24-h LD forcing, i.e. with $x_0 = x_s$. Now consider an arrival HTZ time of X after travel of Z time zones. Upon arrival in the destination time zone, the oscillator will not be entrained to the 24-h LD forcing in the DTZ due to the shift in the LD cycle. For example, consider the blue dots and arrow in Fig. 5. The HTZ arrival time in this case is 11 PM which corresponds to $X = 16$. Therefore $x_s = 16$. The trip consists of travel 11 time zones to the east, $Z = 11$. This corresponds to the vertical blue line and arrow pointing up. In the destination time zone, the DTZ time is 10 AM. Thus the traveler will be subjected to 9 h of light instead of the 8 h of darkness that was expected. Therefore in the DTZ, the oscillator will be phase shifted with regard to the LD cycle and will no longer be entrained. In effect, with regard to the Poincaré section at $X = 16$, the oscillator will have had its initial condition shifted to a new value $x_0 = 3$ and will need to reentrain toward $x_s = 16$. As another example, consider the case of $Z = -8$ and $X = 6$ shown by the red dot and arrow. This depicts travel 8 zones to the west arriving at 1 PM HTZ. The time in the destination zone is 5 AM DTZ. Thus the traveler will be subjected to 2 h of darkness in the destination time zone compared to the 6 h of light that it would have received in the home zone. Now, the oscillator must reentrain to $x_s = 6$ from an initial condition $x_0 = 22$.

We first calculate the reentrainment time by direct simulations assuming a 12:12 LD photoperiod. Define $R = 12 - X - Z$. The quantity R determines how much light or darkness to provide to the oscillator once in the destination time zone until the beginning of the next full 12 h of L or D. In the example of the travel shown in blue, $R = -15$ and we impose 9 h of light followed by 12 h of D. The various cases are summarized below:

- if $R \leq -12$: impose L for $24 + R$, then start 12:12 D:L (eastward travel)
- if $-12 < R \leq 0$: impose D for $12 + R$, then start 12:12 L:D (could be eastward or westward travel)

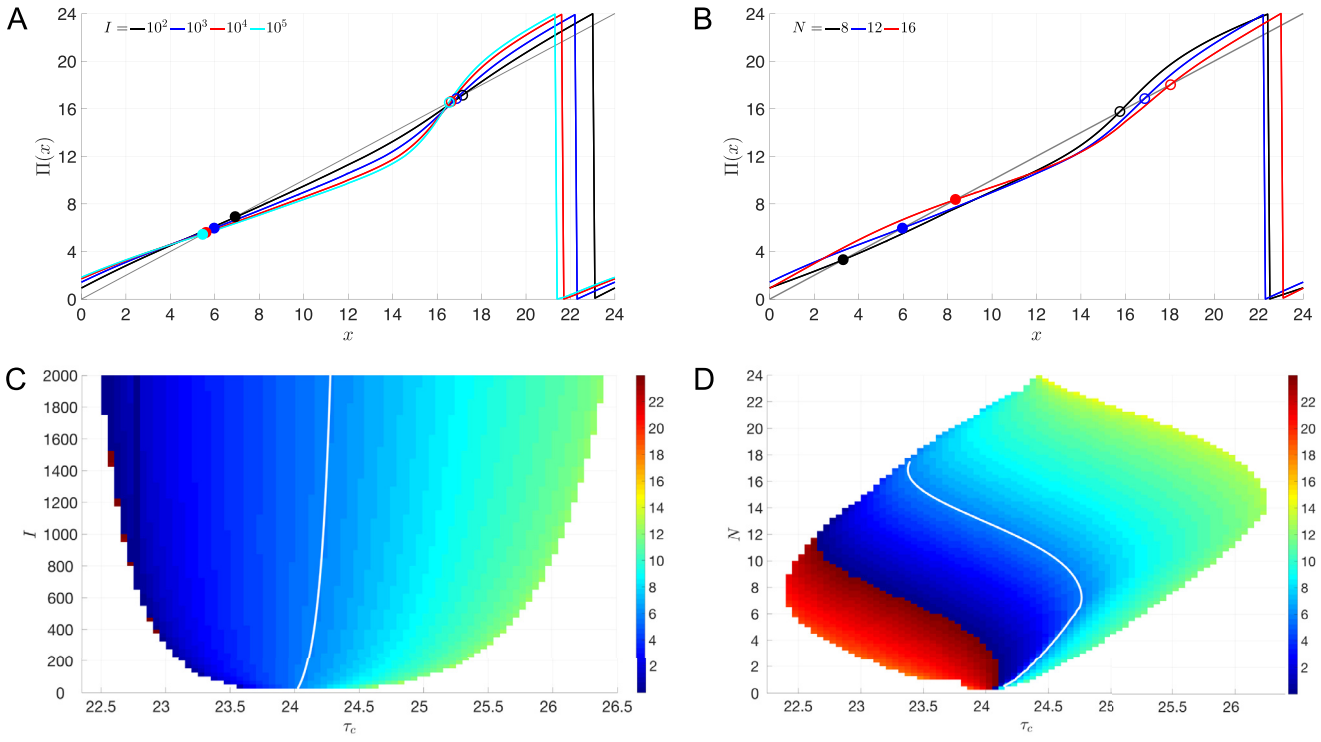

Fig. 4. Dependence of entrainment map on light intensity I and daylength N. (A) Concavity of the entrainment map increases as I is increased, implying that higher light intensity reduces the amount of time it takes an oscillator to reentrain following a phase shift of the LD cycle. The location of the stable fixed points x_s (solid dots) and unstable fixed points x_u (open dots) do not change much as I is varied. For this panel, $\tau_c = 24.2$ h and $N = 12$ h. (B) Stable fixed points of the entrainment map move to the right as N is increased, implying that as daylength increases the phase of entrainment becomes more delayed. The unstable fixed points also move as N is varied. For this panel, $\tau_c = 24.2$ h and $I = 1000$ lux. (C) Arnold tongue computed from entrainment map analysis displaying the entrainment region as a function of τ_c and I. Heatmap colors indicate the location of x_s, i.e. the stable phase of entrainment. The white contour line corresponds to $x_s = 6$. At the borders of the tongue, entrainment is lost through saddle-node bifurcation of x_s and x_u. For this panel, $N = 12$ h. (D) Arnold onion computed from entrainment map analysis displaying stable phases x_s within the entrainment region as a function of τ_c and N. For this panel, $I = 1000$ lux.

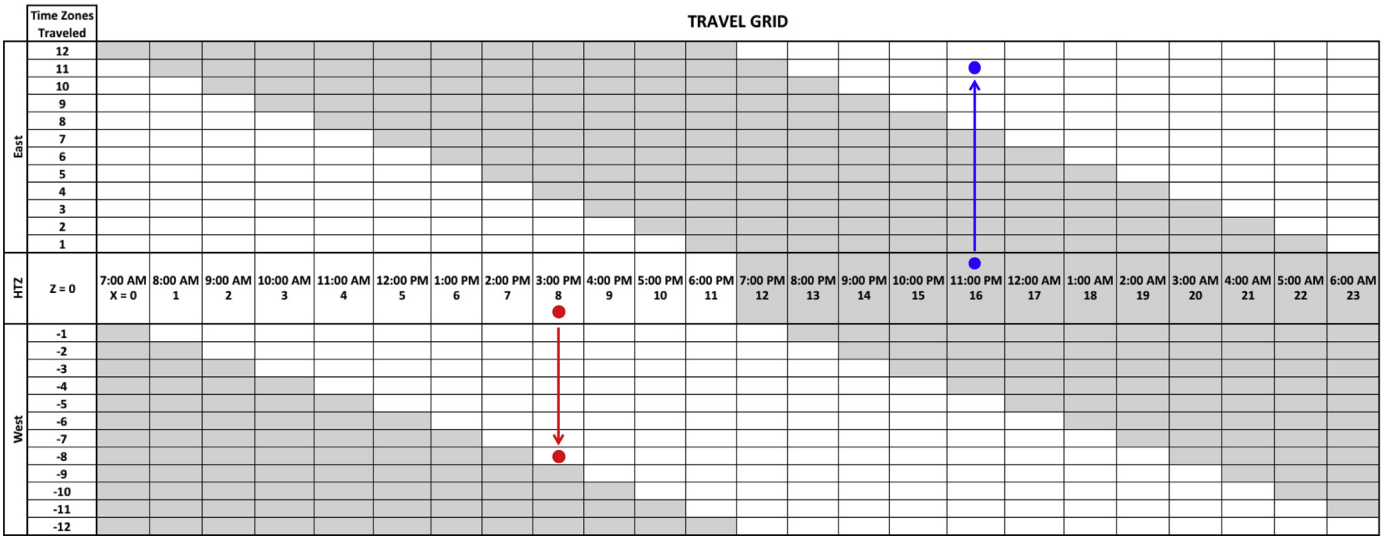

Fig. 5. Schematic diagram of 12:12 LD cycle across all arrival times X and number of time zones traveled Z. This travel grid can be used to easily visualize the offset of the LD cycle due to instantaneous travel and to identify the relationship between the home and destination time zones. The horizontal row in the middle of the grid at $Z = 0$ represents the home time zone (HTZ). The other rows represent destination time zones (DTZs) that lie east (west) for $Z > 0$ ($Z < 0$). The rows are broken up into one hour intervals. The shaded region in each row represents the times of darkness in that time zone relative to HTZ. The Poincaré section $X = 0$ is nominally chosen to correspond to 7 AM HTZ. The blue dots and arrow represent travel 11 time zones east with arrival at 11 PM HTZ and 10 AM DTZ. The red dots and arrow represent travel of 8 time zones west with arrival at 1 PM HTZ and 5 AM DTZ. The entrainment map's arrival time section X is defined with respect to HTZ. (For interpretation of the references to color in this figure legend, the reader is referred to the web version of this article.)

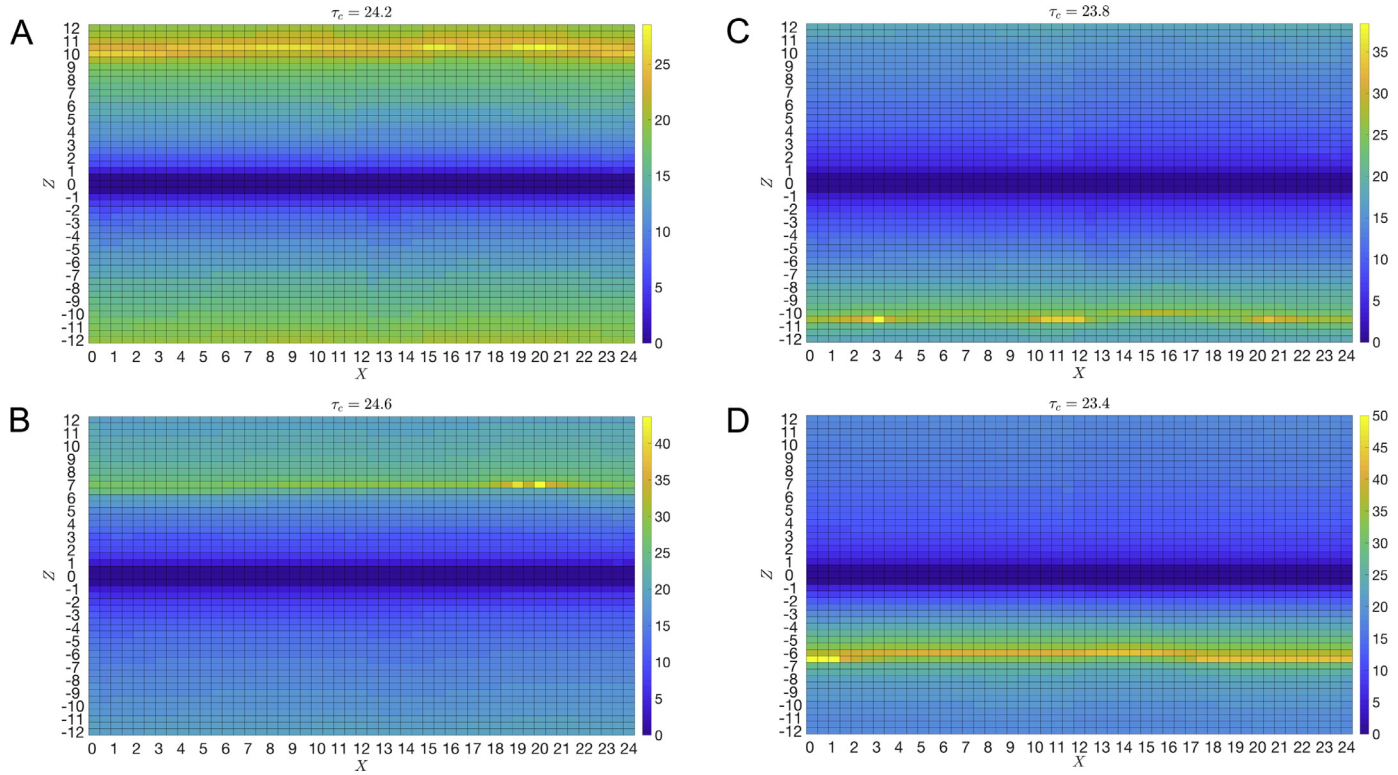

Fig. 6. Reentrainment times and worst-case jet lag from direct simulations across all arrival times X and number of time zones traveled Z. Light colors indicate longer reentrainment times. $Z > 0$ corresponds to eastward travel and $Z < 0$ to westward travel. In these simulations $N = 12$ h and $I = 100$ lux. (A) For the typical human intrinsic period of $\tau_c = 24.2$ h, the longest reentrainment times are for eastward trips of 10.5 time zones ($Z = 10.5$). (B) For a slower than typical intrinsic clock of $\tau_c = 24.6$ h (black), the worst jet lag is for eastward trips of 7 time zones ($Z = 7$). (C) For a faster than typical intrinsic clock of $\tau_c = 23.8$ h, the worst jet lag is westward trips of 10.5 time zones ($Z = -10.5$). (D) For an even faster intrinsic clock of $\tau_c = 23.4$ h, the worst jet lag is for westward trips of 6.5 time zones ($Z = -6.5$).

- if $0 < R \leq 12$: impose L for R, then start 12:12 D:L (could be eastward or westward travel)
- if $12 < R \leq 24$: impose D for $R - 12$, then start 12:12 L:D (westward travel)

With direct simulations, the reentrainment time is calculated from the start of the above procedure until a stopping criterion is achieved; namely, we define reentrainment to have occurred when the magnitude of the time difference between the section crossings of the oscillator and a reference oscillator is less than 0.5 h. The reference oscillator is subjected to the same light-dark protocol as the traveler, but is by definition already entrained to the destination time zone. Thus the reference oscillator starts on the LD-entrained solution at the location given by $(X + Z)$ mod 24.

To calculate the reentrainment time using entrainment maps, at each value X denoting the HTZ arrival time relative to 7 AM, we construct a Poincaré section along the LD limit cycle and define the return map Π_X as before. The fixed point of each map $\Pi_X(x)$ is by definition X. To calculate the appropriate initial condition with which to start iterations in the destination time zone, we determine the new phase relationship between the oscillator and the LD cycle of that time zone. To do so, compute $z_0 = X + Z$. If $0 \leq z_0 < 24$, then choose the initial condition $x_0 = z_0$. If $z_0 > 24$, then $x_0 = z_0 - 24$. If $z_0 < 0$, then $x_0 = z_0 + 24$.

3.3.1. Worst-case travel depends on endogenous period

In Fig. 6, we show entrainment time results over all possible HTZ arrival times (X) and trips (Z) for four different intrinsic periods τ_c. The light intensity was taken at the relatively low level of $I = 100$ lux, which is characteristic of indoor light. Fig. 6A corresponds to the typical endogenous human DD period of 24.2 h. The heatmap shows the reentrainment times with darker colors indicating relatively short reentrainment times, and lighter colors indicating progressively longer times. In each case, the heatmap is asymmetric about $Z = 0$ indicating that reentrainment due to eastward travel can differ compared to westward travel. Indeed, for a $\tau_c = 24.2$ h oscillator, the longest reentrainment times occur for travel roughly 10 and 11 zones to the east. The reentrainment times are relatively insensitive to the arrival time. The remaining panels show the heat maps for different τ_c. For $\tau_c = 24.6$ h (Fig. 6B), the worst trip shifts to smaller values of Z, meaning that shorter eastward trips are more difficult for individuals with slower body clocks. The right column shows the heatmap for individuals whose intrinsic clock is faster than normal, $\tau_c = 23.8$ (Fig. 6C) and 23.4 h (Fig. 6D). Now observe that the worst reentrainment for these individuals occurs for trips to the west, instead of to the east. As the intrinsic clock speeds up, progressively shorter westward trips lead to longer reentrainment. For example at $\tau_c = 23.4$ h, a trip 6 h to the west is the worst.

The entrainment map can be used to explain these findings. In each case, the longest reentrainment time occurs when the travel places the oscillator's initial condition in a neighborhood of the unstable fixed point x_u. The location of x_u relative to x_s depends on τ_c. For example, when $\tau_c = 24.2$ h, we have found that $x_u \approx (x_s + 10.5)$ mod 24, independent of arrival time. Thus travel of 10 or 11 h east would place the initial condition x_0 near the unstable fixed point. Specifically, if the Poincaré section is chosen at X, then $x_s = X$ and $x_u = (X + 10.5)$ mod 24. Travel of $Z > 0$ time zones to the east would imply $x_0 = (X + Z)$ mod 24, therefore $x_0 - x_u = Z - 10.5$. Thus if Z is either 10 or 11, then the initial condition x_0 lies within 0.5 of the unstable fixed point and will lead to very long reentrainment times. This is consistent with the heatmap shown in Fig. 6A.

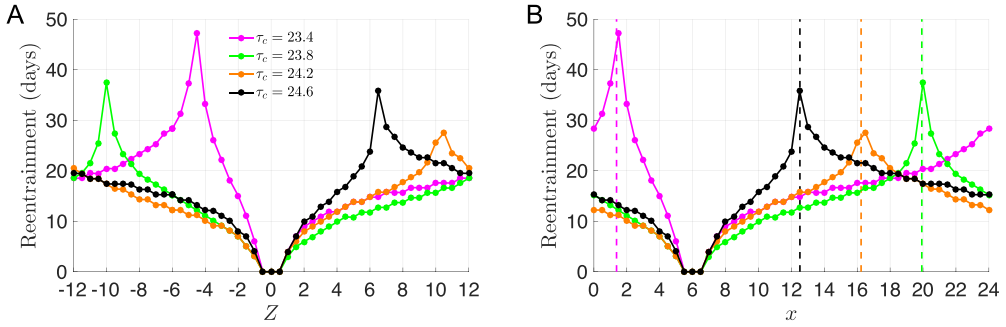

Fig. 7. Worst-case jet lag is explained by the unstable fixed point of the entrainment map. (A) Reentrainment times for the $X = 6$ column of the heatmaps in Fig. 6 (corresponding to an arrival time of 1 PM) computed by cobwebbing the analogous entrainment maps. The longest reentrainment times occur for trips of $Z = -4.5$ for $\tau_c = 23.4$ h (magenta), -10 for $\tau_c = 23.8$ h (green), 10.5 for $\tau_c = 24.2$ h (orange), and 6.5 for $\tau_c = 24.6$ h (black). The reentrainment times and Z value of these local peaks qualitatively agree with the longest reentrainment times found through direct simulation (the yellow hotspots in Fig. 6A–D). (B) Same data as (A), replotted with the horizontal axis in terms of x instead of Z. The local peaks in reentrainment time are at initial conditions near the location of the unstable fixed point x_u (dashed vertical lines) for each value of τ_c, indicating that the worst jet lag occurs after trips that put the traveler in the vicinity of x_u. (For interpretation of the references to color in this figure legend, the reader is referred to the web version of this article.)

Similarly, for different choices of τ_c, we find that the distance between x_u and x_s determines the travel distance and direction that leads to the longest reentrainment time. We illustrate this in Fig. 7 by plotting the reentrainment times derived from cobwebbing the map for a single arrival time $X = 6$, corresponding to one column of the heatmaps. Fig. 7A shows the reentrainment times centered around $Z = 0$ on the horizontal axis. This clearly shows how the worst travel changes as a function of τ_c, and that east-west asymmetry in jet lag exists over all τ_c values chosen. In Fig. 7B, we replot these reentrainment times converting the horizontal axis from Z to x. The dashed vertical lines show the location of x_u for the four different choices of τ_c. Recall that increasing τ_c moves the entrainment map up (Fig. 3B), and causes the unstable fixed point x_u to move to the left. For $\tau_c = 23.4$ h, $x_u \approx 1.5$ (dashed magenta line), and as τ_c increases x_u moves to the left through the $x = 0$ boundary and emerges through the $x = 24$ boundary at progressively leftward values (green, orange and black dashed lines). The longest reentrainment times predicted by the map are for travel of Z time zones that places the initial condition x_0 near x_u in each of these four cases. To find the worst-case trip, we find the value of $Z_D \in (-12, 12)$ that solves $x_u = (x_s + Z_D)$ mod 24. In all cases the arrival time was held fixed at $X = 6$, implying $x_s = 6$. From the map, we found the values x_u to approximately equal 12.5, 16.5, 20, and 1.5 for $\tau_c = 24.6$, 24.2, 23.8, and 23.4 h, respectively. Solving for the corresponding Z_D values yields 6.5, 10.5, -10, and -4.5 respectively. These correspond to the worst possible trips being 6 h east, 10.5 h east, 10 h west, and 4.5 h west respectively, which are qualitatively consistent, and except for $\tau_c = 23.4$ h, quantitatively consistent with the reentrainment time heatmaps from direct simulation (Fig. 6). We call Z_D a *demarcation point*, since it separates trips that reentrain through phase advance or phase delay. Its properties will be further discussed in Section 3.5.

Fig. 6 indicates that the average amount of time it takes to reentrain after travel also depends on τ_c. For example, consider the 49 possible trips represented by $Z \in (-12, 12)$ in increments of 0.5, with the arrival time held fixed at $X = 6$. The median reentrainment times for these trips with $\tau_c = 24.6$, 24.2, 23.8, and 23.4 h are 16.3, 13.3, 13.2, and 17.6 days, respectively. The longer median reentrainment times correspond to τ_c values closer to the bifurcation points at which entrainment is lost. Maps that are closer to bifurcation have less concavity, and therefore longer reentrainment times (Fig. 4A and Diekman and Bose, 2016). This finding is consistent with previous work showing that for a variation of the Poincaré oscillator, reentrainment times are longer near the borders of the Arnold tongue entrainment region than at the center (Granada and Herzel, 2009).

3.3.2. Quantifying the east-west asymmetry of jet lag

Fig. 8 shows a comparison of reentrainment times calculated using the map (empty circles) versus direct simulation (filled circles). In each case, the Poincaré section was chosen at $X = 6$. Reentrainment times for trips to the east (west) are shown in blue (red). The qualitative predictions of the entrainment map match those from the direct simulations. First, both methods show that trips to the east require longer reentrainment times than trips to the west for humans with average to slow body clocks. This is evidenced by the blue curves lying above the red curves in the two panels in the left column. The opposite is true for humans with fast body clocks as shown in the right column. These plots show that the extent of the east-west asymmetry found in reentrainment times depends critically on the endogenous period of the underlying DD oscillator. Second, the two methods yield results that are in very close agreement for westward travel of travelers with average to slow body clocks (Fig. 8A and B, red) and eastward travel for fast body clocks (Fig. 8C and D, blue). For travel in the opposite directions than these, the two methods quantitatively agree over many time zones, but there are intervals where they disagree. The place where the two methods quantitatively differ is when traveling to a time zone that lies in a neighborhood of the unstable fixed point. The predictions from the map for reentrainment for initial conditions that lie arbitrarily close to the unstable fixed point can become arbitrarily large. This is a consequence of the structure of piecewise monotone maps and the particular details of the entrainment map for FJK model. An arbitrarily large number of iterates are needed to leave a neighborhood of x_u if x_0 is chosen sufficiently close to it. In general, this leads to a map-based prediction that is larger than what is found in direct simulations, as seen by the larger peaks in the dashed curves than the solid curves in Fig. 8. In addition, for $\tau_c = 24.6$ and 23.4 h, the map-based predictions of the Z value corresponding to the worst-case reentrainment time are quantitatively different than the results from direct simulation (6.5 versus 7 h East for $\tau_c = 24.6$ h, and 4.5 versus 6 h West for $\tau_c = 23.4$ h), as further discussed in the Appendix.

Despite these differences, the map is useful to draw several conclusions. First, the sign and magnitude of the difference $x_u - x_s$ determines which direction of travel and over how many time zones leads to the worst jet lag. For those with a normal to slow intrinsic period, travel to the east will lead to the worst jet lag because the unstable fixed point x_u lies to the right of the stable one x_s. For those with a faster than normal intrinsic period, it is travel to the west that will lead to the worst jet lag. Second, the proximity of the initial condition x_0 in the destination time zone to x_u determines, in part, the length as well as the direction of reentrain-

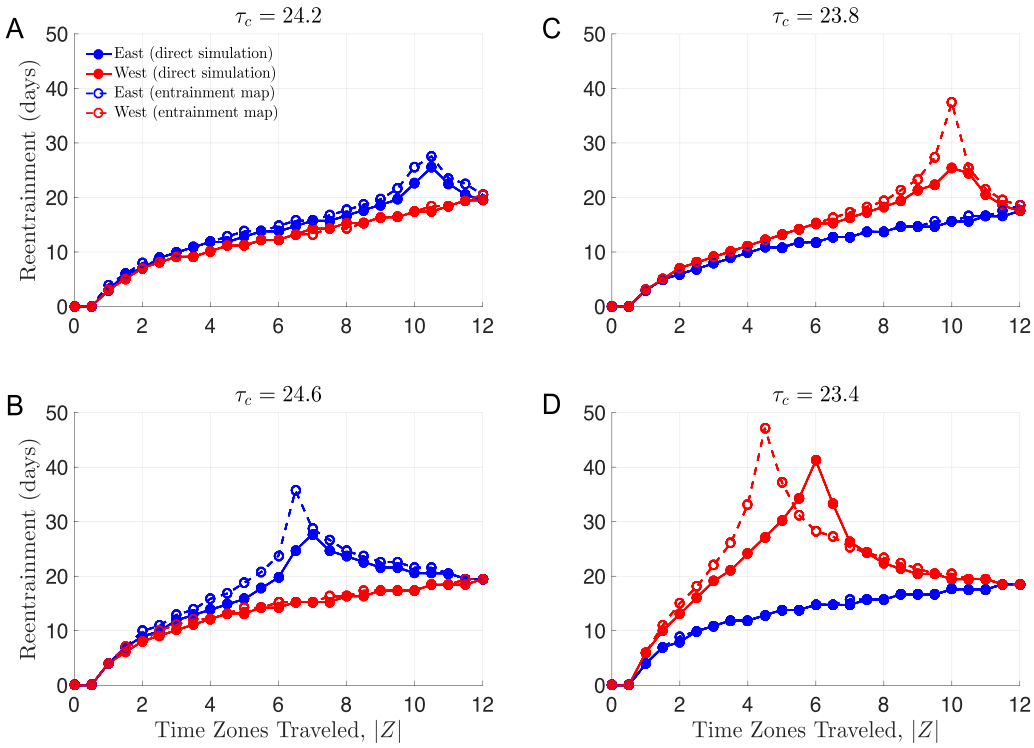

Fig. 8. East-West asymmetry of reentrainment times depends on intrinsic period τ_c. The reentrainment times for an arrival time of 1 PM obtained through direct simulation (solid lines and filled dots) qualitatively agree with the reentrainment times obtained by cobwebbing the analogous entrainment maps (dashed lines and open circles). (A) For $\tau_c = 24.2$ h, eastward trips (blue) take longer to reentrain from than westward trips (red). (B) For $\tau_c = 24.6$ h, eastward trips are worse than westward trips as in (A) but here the degree of asymmetry is increased. (C) For $\tau_c = 23.8$ h, westward trips take longer to reentrain from than eastward trips. (D) For $\tau_c = 23.4$ h, westward trips are worse than eastward trips as in (C) but here the degree of asymmetry is increased. (For interpretation of the references to color in this figure legend, the reader is referred to the web version of this article.)

ment (either through phase advance or delay). Since reentrainment times are quite sensitive to initial conditions in a neighborhood of x_u, we are hesitant to attribute too much importance to very long reentrainment times. We will further study the role of x_u in determining the direction of reentrainment in Section 3.3.3.

3.3.3. Orthodromic versus antidromic reentrainment

We now address the direction of reentrainment, and in particular the circumstances that lead to orthodromic versus antidromic reentrainment. Fig. 9 shows the regions of orthodromic and antidromic reentrainment for the four different choices of τ_c. For $\tau_c = 24.2$ h, antidromic reentrainment occurs when travel to the east causes the initial condition to lie in the interval $(x_u, 18)$. The lower bound of x_u is necessary to place the initial condition on the "opposite" side of x_u. The upper bound of 18 reflects that 12 is the maximum number of zones of eastward travel ($x_s + 12 = 18$). In this case, $x_u = 16.5$ and eastward trips of 10.5 zones or greater lead to antidromic reentrainment. All other trips in either direction are followed by orthodromic reentrainment (Fig. 9A). As τ_c increases to 24.6, the unstable fixed point x_u moves to the left, thus creating a larger interval $(x_u, 18)$ of antidromic reentrainment (Fig. 9B). The case for $\tau_c = 23.8$ h (Fig. 9C) is largely the same as $\tau_c = 24.2$ h, except that antidromy occurs for westward trips of 10 to 12 zones when x_0 lies in the interval $(18, x_u)$. For $\tau_c = 23.4$ h (Fig. 9D), x_u has moved to right, through the boundary at $x = 24$ to about 1.5. Thus the region of antidromy is the union of the intervals $(0, x_u)$ and $(18, 24)$. To summarize, antidromic reentrainment can occur when the number of time zones traveled is larger than the distance between x_s and x_u.

Antidromic reentrainment is typically regarded as leading to longer reentrainment times than orthodromic reentrainment (Arendt et al., 1987; Klein and Wegmann, 1977; Sack, 2010). Our results suggest that while this is often true, it is not always the case. For example, consider eastward trips of 10 and 11 time zones for the $\tau_c = 24.2$ h oscillator with an arrival time of $X = 6$. The $Z = 10$ trip corresponds to $x_0 = 16$ and entrains orthodromically, whereas the $Z = 11$ trip corresponds to $x_0 = 17$ and entrains antidromically (Fig. 9A). In this case the orthodromic reentrainment takes longer (27.5 days) than the antidromic reentrainment (22.5 days); to see this compare the $Z = 10$ and $Z = 11$ data points in Fig. 7A. Furthermore, this orthodromic $Z = 10$ trip also has a longer reentrainment time than the corresponding 10-zone eastward trip for $\tau_c = 24.6$ h, which reentrains antidromically (21.5 days); to see this compare the orange and black $Z = 10$ data points in Fig. 7A. The possibility of antidromic reentrainment being faster than orthodromic reentrainment was also noted in a molecular model of the mammalian circadian clock (Leloup and Goldbeter, 2013). This feature is due to x_u creating a boundary that separates the x_0 values that reentrain through phase advances from those that reentrain through phase delays, and the fact that reentrainment times are sensitive to the distance between x_0 and this boundary.

To better understand the effect of photoperiod and intrinsic period on orthodromy/antidromy, we computed the differences in reentrainment times for the specific cases of trips made 10 time zones to the east and west ($|Z| = 10$) over a range of N and τ_c values. To simplify the argument, we choose the Poincaré section to lie at $X = 12$ for the different LD-entrained solutions that we will consider. This implies that $x_s = 12$. Antidromic reentrainment can only occur when the distance between x_s and x_u is less than 12. In Fig. 10 we show a heat map derived from cobweb simulations for trips 10 h to the east and west. We plot the difference of reentrainment times (east minus west). There are three principal features of this heat map. First is the solid black curve, which we call the *neutral period curve* for $|Z| = 10$, or NPC_{10}. The neu-

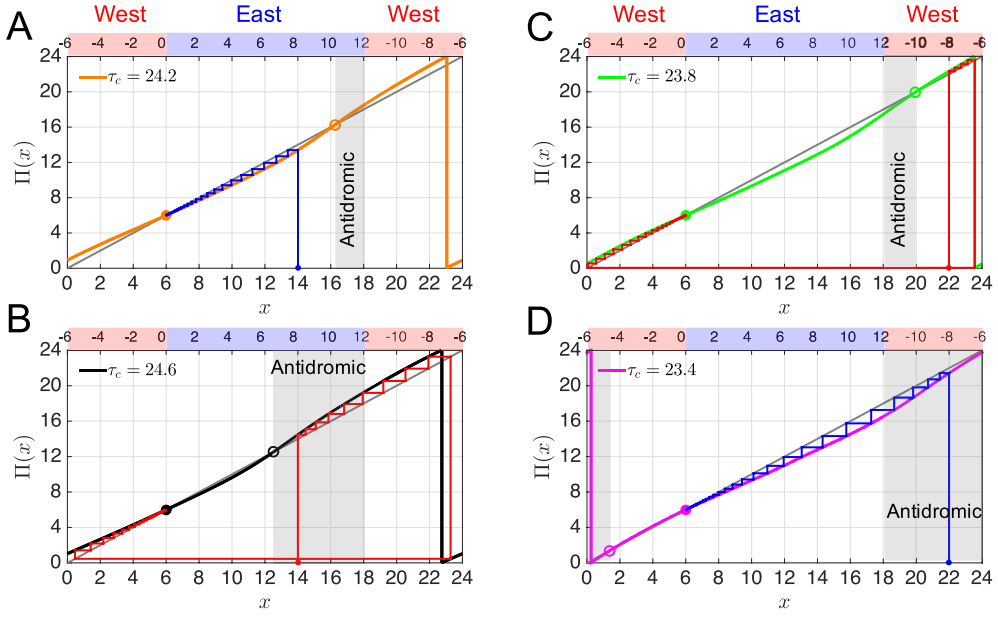

Fig. 9. Unstable fixed point of entrainment map controls whether reentrainment is orthodromic or antidromic. (A) After traveling 8 time zones east (a phase advance of the LD cycle), reentrainment occurs through phase advances and is therefore orthodromic if $\tau_c = 24.2$ h. The reentrainment time is 17.69 days. (B) The same trip as in (A) reentrains through phase delays and is therefore antidromic if $\tau_c = 24.6$ h. The reentrainment time is 24.64 days. (C) After traveling 8 time zones west (a phase delay of the LD cycle), reentrainment occurs through phase delays and is therefore orthodromic if $\tau_c = 23.8$ h. The reentrainment time is 19.31 days. (D) The same trip as in (C) reentrains through phase advances and is therefore antidromic if $\tau_c = 23.4$ h. The reentrainment time is 23.35 days.

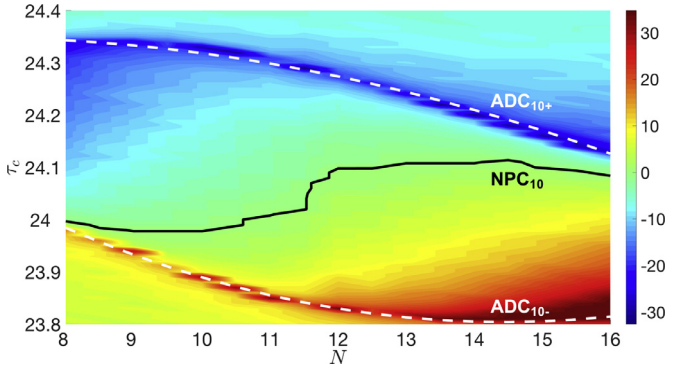

Fig. 10. East-West asymmetry and antidromic reentrainment depend on daylength N. Reentrainment times were determined by cobwebbing entrainment maps for eastward and westward trips of 10 time zones ($Z = \pm 10$) over a range of N and τ_c values with $I = 100$ lux and the stable fixed point held at $x_s = 12$. The colormap represents the degree of asymmetry in reentrainment times in units of days, and was calculated by subtracting the reentrainment time for $Z = 10$ from the reentrainment time for $Z = -10$. Therefore negative values correspond to (N, τ_c) pairs for which eastward travel is worse, and positive values to westward travel being worse. Along the black neutral period curve (NPC_{10}), reentrainment times are the same for eastward and westward travel. Along the upper dashed white curve (ADC_{10^+}), the unstable fixed point is 10 h to the right of x_s, i.e. $x_u = 22$. Along the lower dashed white curve (ADC_{10^-}), the unstable fixed point is 10 h to the left of x_s, i.e. $x_u = 2$. In between these antidromy curves all reentrainment is orthodromic; outside these curves all reentrainment is antidromic. Note that eastward travel is much worse than westward travel (dark blue colors) near ADC_{10^+}, whereas westward travel is much worse than eastward travel (dark red colors) near ADC_{10^-}. (For interpretation of the references to colour in this figure legend, the reader is referred to the web version of this article.)

tral period curve is a generalization of the concept of neutral period introduced by Aschoff et al. (1975). Points on NPC_{10} represent (N, τ_c) parameter pairs for which the reentrainment time after a trip 10 time zones east is identical to the reentrainment times for 10 zones to the west. For any parameter values that lie above the NPC_{10}, trips of 10 zones to the east are worse than 10 zones to the west. The other two important features of Fig. 10 are the dark blue and red regions of the heat map. These lie in a neighborhood of what we call the ADC_{10^+} and ADC_{10^-} antidromy curves. These curves correspond to parameter values at which $x_u - x_s = 10$ or -10 respectively. For parameter values that lie near ADC_{10^+} (ADC_{10^-}), trips 10 zones to the east (west) place the initial condition for reentrainment very close to the unstable fixed point x_u. Reentrainment times calculated from the map for such initial conditions are arbitrarily long. For parameter values between the two antidromy curves, reentrainment after a trip of 10 time zones is always orthodromic. But for eastward trips made with parameter values above the ADC_{10^+}, reentrainment is antidromic. While for westward trips made with parameters below the ADC_{10^-} curve, reentrainment is antidromic.

By studying a fixed horizontal slice of Fig. 10, we can compare how a traveler's reentrainment times can differ as a function of the time of the year. For example, during the summer months the value N in the photoperiod is larger than 12, while during the winter it is less than 12. Thus the left $N = 8$ h edge of the graph corresponds to reentrainment during the winter and the right edge at $N = 16$ h corresponds to reentrainment during the summer. Consider the $\tau_c = 24.2$ h slice which shows that traveling east will be worse than west at all times of the year. The asymmetry is greater in the summer than in the winter. Furthermore in winter the reentrainment will be orthodromic; the parameter pair (8, 24.2) lies below ADC_{10^+}. In summer it will be antidromic; the parameter pair (16, 24.2) lies above ADC_{10^+}. For a person with a slower body clock, e.g. $\tau_c = 24.3$ h, eastward travel is still worse than westward all year-round and reentrainment is still orthodromic in winter and antidromic in summer, but now the east/west asymmetry is more severe in winter than summer. For someone with a fast body clock, e.g. $\tau_c = 23.9$ h, west is always worse than east, but more so in summer than winter. Here, reentrainment is antidromic in winter (since (8, 23.9) lies below ADC_{10^-}), and orthodromic in summer (since (16, 23.9) lies above ADC_{10^-}), which is the opposite relationship between season and the type of reentrainment as the other two τ_c values considered.

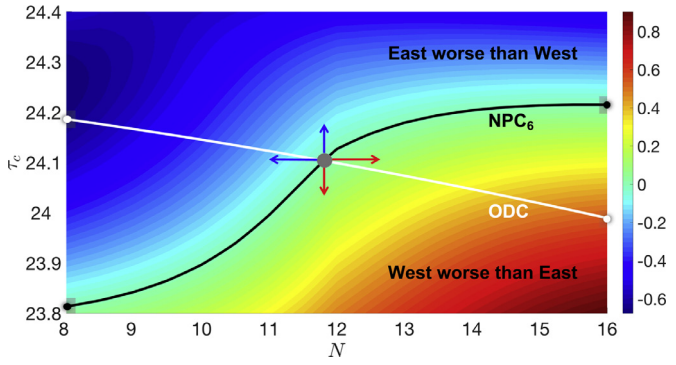

Fig. 11. East-West asymmetry persists in the absence of antidromic reentrainment. For entrainment maps over a range of N and τ_c values with $I = 100$ lux and the stable fixed point held at $x_s = 12$ (same maps as in Fig. 10), the first iterate of the maps was used as a surrogate for the reentrainment time following eastward and westward trips of 6 time zones ($Z = \pm 6$). The colormap represents the degree of asymmetry in the first iterate, and was calculated by subtracting $\Delta_{N,\tau_c}(6)$ from $\Delta_{N,\tau_c}(18)$; see text for definition of $\Delta_{N,\tau_c}(x_0)$. Negative values correspond to (N, τ_c) pairs for which eastward travel is worse, and positive values to westward travel being worse. Along the black neutral period curve (NPC_6), $\Delta_{N,\tau_c}(6) = \Delta_{N,\tau_c}(18)$ implying reentrainment times are the same for eastward and westward travel. Along the white orthodromy curve (ODC), the unstable fixed point is 12 h away from x_s (i.e. $x_u = 0 = 24$), and all reentrainment is orthodromic. At the intersection of the ODC and NPC_6 (the gray dot), reentrainment is both orthodromic and east-west symmetric. From this intersection point, increasing (decreasing) τ_c or decreasing (increasing) N introduces an asymmetry leading to worse jet lag for eastward (westward) travel; see text for a detailed explanation of this phenomenon based on properties of the entrainment map.

Note that the axes of the heatmap shown in Fig. 10 are τ_c and N, which are the same two parameters as the axes of the Arnold onion in Fig. 4D (albeit with the axes reversed). These two figures convey different information however. The Arnold onion shows how the stable entrained phase x_s changes with parameter variations. It does not contain information about the transient time it takes for trajectories to converge to the stable phase. The heat map in Fig. 10, on the other hand, is constructed so that the stable phase is always at x_s=12 for all parameter pairs. Thus it does not contain meaningful phase of entrainment information, but instead provides valuable information about reentrainment times.

3.4. Explaining the east-west asymmetry

As above, choose the Poincaré section to lie at $X = 12$ for the different LD-entrained solutions. Since x_s is fixed at 12, we can vary the location of x_u by changing τ_c and/or N. In general, increasing τ_c makes x_u decrease, while decreasing N makes x_u increase. By balancing N and τ_c appropriately, we define the *orthodromy curve* (ODC) as a monotone decreasing curve in $N - \tau_c$ space along which the distance $|x_u - x_s| = 12$; see the white curve in Fig. 11. To find this curve, we chose the values $N = 8$, 12, and 16 h and computed the corresponding τ_c values that led to $|x_u - x_s| = 12$. We then fit a quadratic curve through the ensuing three ordered pairs (the white and gray dots in Fig. 11); the resulting curve is quite linear, suggesting that three points is sufficient for approximating the shape of the ODC. The importance of the ODC is that an oscillator with parameters (N, τ_c) of a point chosen along the ODC can only experience orthodromic reentrainment, since it is not possible for a 12-h trip leaving from x_s to go beyond x_u in either direction.

Next we focus on six hour trips in either direction. We will use the first iterate of the entrainment map to help determine whether reentrainment after travel to the east is faster or slower than after travel to the west. Define $\Delta_{N,\tau_c}(x_0) = |\Pi(x_0) - x_0|$. This is the distance of the entrainment map from the diagonal for trips with initial condition x_0 for the choice (N, τ_c). It measures the amount of phase advance or delay on the first iterate. A larger value indicates a greater amount of phase change. We have found that a larger initial phase change ultimately leads to *shorter* reentrainment times. We shall use $\Delta_{N,\tau_c}(x_0)$ as a surrogate for comparison of actual reentrainment times. An eastward trip of 6 h corresponds to $x_0 = 18$ and a 6 h westward trip corresponds to $x_0 = 6$. Thus our convention is that for a particular ordered pair (N, τ_c), if $\Delta_{N,\tau_c}(6) < \Delta_{N,\tau_c}(18)$, then reentrainment after a trip to the west is longer. If the inequality is switched, trips to the east lead to longer reentrainment.

Using this convention and computing at the left endpoint of the ODC, we find $\Delta_{8,\,24.1683}(6) > \Delta_{8,\,24.1863}(18)$. This implies that an eastward trip of 6 h is followed by longer reentrainment compared to a westward trip of 6 h. At the right endpoint of the ODC, we find that $\Delta_{16,\,23.9893}(6) < \Delta_{16,\,23.9893}(18)$ implying that westward trips take longer to reentrain from. By continuously varying N and τ_c along the ODC, there exists a unique value, found to be $N = 11.8116$, $\tau_c = 24.1035$, at which $\Delta_{11.8116,24.1035}(6) = \Delta_{11.8116,24.1035}(18)$, i.e. the distance from the map to the diagonal is the same for $x_0 = 6$ and 18. We call this a neutral period point since it is a combination of photoperiod and intrinsic period for which reentrainment times are the same for the pair of initial conditions that lie a symmetric distance of 6 h away from the stable fixed point $x_s = 12$; see the gray dot in Fig. 11. We next computed the neutral period points along the vertical edges of the parameter space, finding them to be at $N = 8$, $\tau_c = 23.8133$ and $N = 16$, $\tau_c = 24.2147$ (black dots in Fig. 11). Since the maps depend continuously on N and τ_c, there exists a neutral period curve, NPC_6, in the $N - \tau_c$ space, that passes through these three neutral period points, along which 6 h trips in either direction lead to the same reentrainment time as determined from the condition $\Delta_{N,\tau_c}(6) = \Delta_{N,\tau_c}(18)$; see the black curve in Fig. 11.

The neutral period curve NPC_6 divides the parameter space into two distinct regions. Above NPC_6 (such as at the left endpoint of the ODC), reentrainment after eastward trips takes longer. Below NPC_6 (such as at the right endpoint of the ODC), reentrainment after westward trips takes longer. Note that NPC_6 must lie below the ODC for $N < 11.8116$ and above the ODC for $N > 11.8116$. To understand why, consider the neutral period point on the ODC where $N = 11.8116$, $\tau_c = 24.1035$. At this point $\Delta_{11.8116,24.1035}(6) = \Delta_{11.8116,24.1035}(18)$. Now consider a value of the parameters with the same N value but larger τ_c value. Since the entrainment map moves up as τ_c increases, the value $\Pi(6)$ will shift further away from the diagonal while the value $\Pi(18)$ will shift closer to the diagonal. This immediately implies for all $\tau_c > 24.1035$ that $\Delta_{11.8116,\tau_c}(6) > \Delta_{11.8116,\tau_c(18)}$, which implies that eastward travel is worse. Thus all such parameter pairs must lie on the same side of neutral period curve as the left endpoint of the ODC. Alternatively, for $\tau_c < 24.1035$, the map $\Pi(x)$ shifts down and $\Delta_{11.8116,\tau_c}(6) < \Delta_{11.8116,\tau_c}(18)$; westward travel is worse and all these parameter pairs must lie on the same side of NPC_6 as the right endpoint of the ODC. Together, this implies the following relationship between NPC_6 and the ODC: to the left of the intersection point of NPC_6 and the ODC, NPC_6 must lie below the ODC; whereas to the right of their intersection point, NPC_6 must lie above the ODC.

Several observations are in order. First, since NPC_6 intersects the ODC, our results show that east-west asymmetry does not require antidromic reentrainment. Indeed, along the ODC, all trips have orthodromic reentrainment. Roughly half of this curve lies to the left of the NPC where east is worse and the other to the right where west is worse. The results suggest that east-west asymmetry is a natural feature of the FJK model. Second, by considering various horizontal slices of the $N - \tau_c$ plane shown in Fig. 11 for fixed values of τ_c, we see that the duration of light N in the photoperiod is crucial for determining the direction and extent of asymmetry. In particular, as N is increased, westward travel takes increasingly longer to recover from. This suggests that, for example, individuals

with fast clocks will experience more jet lag after eastward trips than westward trips in the winter, whereas during the summer westward trips are worse. On the other hand, for individuals with slow clocks, eastward trips cause more jet lag than westward trips at all times of the year, since horizontal lines above $\tau_c = 24.2$ h lie to the left and above NPC_6 for all N.

3.5. Fast reentrainment and the phaseless set

Numerous experiments and models have found that a stimulus of a critical strength applied at a critical phase can suppress the amplitude of a circadian oscillator to nearly zero (Jewett et al., 1991; Sun et al., 2016; Ukai et al., 2007; Winfree, 1970). It has been suggested that driving the oscillator to this phaseless position, referred to as the "singularity", could shorten reentrainment time by allowing the trajectory to take a "shortcut" in phase space (Serkh and Forger, 2014; Winfree, 1991). We show that in the FJK model, this shortcut can arise at both low and high light intensities. We will use the entrainment map to locate a set of initial conditions (critical phases) that allow trajectories to take this shortcut. For higher light intensities, this shortcut can be accessed from points on the LD-entrained solution by changing the light offset x by an appropriate amount, which can give rise to unusually fast reentrainment.

Consider higher intensity light with $I = 1000$ lux. In Fig. 12A, we reconstruct the heat map for $\tau_c = 24.2$ h using direct simulation. In comparison to Fig. 6A, note that now there is a band near $Z = 10$ and $Z = 11$ for which reentrainment times are much shorter than for nearby Z values. These are examples of trips for which reentrainment is much faster than would be expected. In addition, note that within this band, reentrainment depends on the arrival time much more sensitively than for the $I = 100$ lux case. For example, for $Z = 10$ arrival times near 7 AM incur shorter reentrainment than others. For $Z = 10.5$, arrival times from 12:30 PM to 5:30 PM have shorter reentrainment, while for $Z = 11$, arrival from 11:00 PM to 1:30 AM have quite short reentrainment times.

Recall the definition of the demarcation point $Z_D \in (-12, 12)$ which solves $x_u = (x_s + Z_D) \mod 24$. For $\tau_c = 24.2$, $Z_D = 10.67$ as the unstable fixed point lies roughly 10.67 time zones to the east of the stable one. The demarcation point Z_D lies in the band of fast entrainment. Consider the Poincaré map fixed at $X = 6$ (1:00 PM), which has $x_s = 6$ and $x_u = 16.67$. Fig. 12B shows entrainment times for the $X = 6$ vertical column of the heat map, centered around $Z = 0$. Note that as $|Z|$ increases, entrainment times increase as would be predicted from the map. However as Z increases through 10, entrainment times suddenly begin to dip, reaching a local minimum at $Z = 10.46$ (which is near Z_D), then increasing until $Z = 11$ before beginning to fall again (gray shaded region of figure). The entrainment map predicts instead that the reentrainment times would show a local maximum, not a local minimum, in this neighborhood. In contrast, with $I = 100$ lux both the map and simulations show a local maximum in this neighborhood (Fig. 8A), which is why we chose to work with that light level in Sections 3.3 and 3.4.

To explain why there is fast entrainment, we identify a region of phase space that Guckenheimer (1975) calls a *phaseless set*. The easiest way to describe this set is to consider an unforced oscillator, say with $n \equiv 0$ which gives rise to the stable DD limit cycle. Every point on the DD limit cycle can be assigned a phase between 0 and τ_c. Now consider the $A - C$ phase plane. Following (Guckenheimer, 1975), we define a point to be phaseless if every neighborhood of that point intersects each isochron of the stable DD limit cycle. An isochron consists of the set of initial conditions that have the same asymptotic phase as a particular point on the DD limit cycle. In particular, two nearby initial conditions that lie in the phaseless set can have very different asymptotic phases. The phaseless set lies in a region of phase space where the isochrons meet to form a pinwheel or a singularity. For any fixed value of n in the FJK model, including $n = 0$ (DD) or $n = 1$ (LL), this singularity lies in a neighborhood of the origin in $A - C$ space. A tubular neighborhood of the origin extending in the n direction can be considered as the generalization of the phaseless set for the periodically LD-forced FJK model. Trajectories that pass through this set deviate from the usual dynamics in that they do not stay close to the LL and DD limit cycles during the reentrainment process. Instead they take the aforementioned shortcut across phase space during reentrainment. Characteristics of these trajectories include amplitude suppression, an inability to predict whether the entrainment is strictly through advance or delay, and situations in which the phase of the trajectory cannot be clearly discerned on a cycle-by-cycle basis. What we have found in simulation is that travel to time zones in a neighborhood of the demarcation point Z_D, equivalently choosing an initial condition on the Poincaré section near x_u, leads to trajectories that enter the phaseless set and take a shortcut across phase space.

Fig. 12C–F shows the reentrainment process for the trajectories whose initial conditions lie in a neighborhood of x_u, $x_0 = 16.46$ (Panels C and D) and $x_0 = 16.68$ (Panels E and F). Both trajectories show amplitude suppression and take a shortcut across the projection onto the $A - C$ phase space; Panels C and E. The green dots in each of those panels indicate where the lights turned on in the current LD cycle. By the 4th cycle, both trajectories have reached a region of maximal suppression, but at the 5th cycle, the trajectory in Panel C emerges from that region in such a way that it quickly entrains to the correct phase (as shown by the red dot(s) on each of the panels). The trajectory in Panel E does not. From Panel D, one could argue that the trajectory entrains through phase advancing, but the entrainment in Panel F defies such characterization. In particular, the phase of this trajectory does not appear to be predictable on a cycle-by-cycle basis. What is common to the two trajectories in Panels D and F is that prior to entering the region of amplitude suppression (phaseless set), neither one seems to be systematically phase advancing or delaying. We comment further on this in the Appendix, where we show that a shortcut also exists in phase space at lower light intensities, but that this shortcut is not directly accessible through travel.

3.6. Jet lag due to north-south travel

The question of whether jet lag occurs due to north-south travel has received very little attention. Here we show that in fact there can be jet lag effects following long-distance north-south travel due to significantly different photoperiods between the departure and arrival locations. We show that these effects depend on the intrinsic period τ_c of the traveler, and that the direction of reentrainment (phase advance or phase delay) can be considered analogously to orthodromic and antidromic reentrainment due to east-west travel.

In modeling north-south travel and subsequent reentrainment, let N_{dep} be the number of hours of light in the departure city and N_{dest} be the number of hours of light in the destination city. We will make the following assumptions:

- Prior to and during the flight, the traveler remains entrained to the departure LD cycle ($N = N_{dep}$).
- Upon arrival at the destination, the traveler lies on a Poincaré section that intersects the LD-entrained solution ($N = N_{dep}$) of the departure city X_{dep} hours after the lights turned on in the departure city.
- This Poincaré section intersects the LD-entrained solution ($N = N_{dest}$) of the destination city at a location X_{dest} hours after the lights last turned on in the destination city.

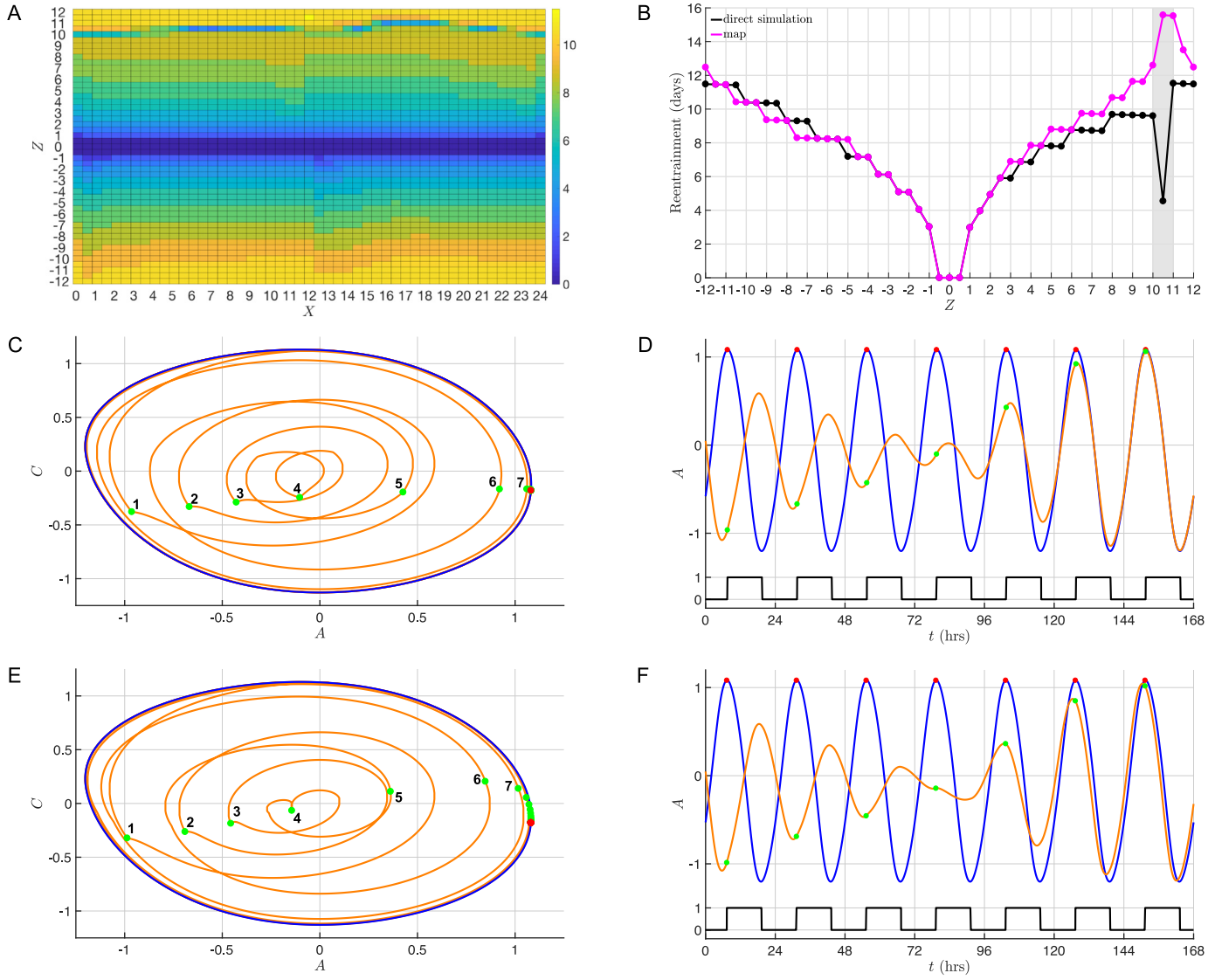

Fig. 12. Dramatically short reentrainment times are possible for travelers entering the phaseless set. (A) Heatmap of direct simulation reentrainment times (in days) for arrival times X and trips Z with $\tau_c = 24.2$ h, $N = 12$ h, and $I = 1000$ lux. There is a local minimum for eastward trips of 10.5 h ($Z = 10.5$). (B) Reentrainment times for $X = 6$ from direct simulation (black) and from cobwebbing the corresponding maps (magenta). The local minimum of reentrainment time observed in direct simulation corresponds to a local maximum predicted by the map, and occurs for trips that place the traveler in a region near the unstable fixed point of the map called the phaseless set (gray shading). (C–D) Phase plane trajectory (C) and time course (D) during reentrainment for $Z = 10.46$, which exhibits amplitude suppression and very fast reentrainment (4.5 days) for the traveler (orange). The green dots correspond to the location of the traveler when the lights turn on ($x = 0$), with labels indicating the first 7 cycles. The red dot is $x = 0$ for the reference oscillator (blue trajectory). (E-F) Phase plane trajectory (E) and time course (F) during reentrainment for $Z = 10.68$, which exhibits amplitude suppression but does not lead to very fast reentrainment (9.5 days). (For interpretation of the references to colour in this figure legend, the reader is referred to the web version of this article.)

- Upon arrival, in direct simulation, the traveler is subjected to the appropriate amount of light and/or dark to complete the current 24 h cycle and is then subjected to the destination LD cycle ($N = N_{dest}$).
- Upon arrival, the entrainment map is based on the Poincaré section X_{dest} and reentrainment time is calculated with an appropriate initial condition as described below.

To illustrate our findings we will work with a specific example: travel between New York City and Santiago, Chile on the Northern hemisphere's summer solstice. The reason for this choice is that at this time of the year, both cities lie in the same time zone and we do not have to adjust for east-west shifts. Below we will refer to the NYC LD-entrained solution and the Santiago LD-entrained solution. These solutions occur in our model for LD photoperiods of 15:9 ($N = 15$ h) and 10:14 ($N = 10$ h) respectively, with $I = 1000$ lux. This light intensity is characteristic of outdoor light and provides a wider range of entrainment in τ_c than does 100 lux (Fig. 4C), which makes it easier to illustrate some of our findings in Sections 3.6 and 3.7.

On the northern solstice (June 20, 2016), the sun rose at 5:25 AM and set at 8:31 PM in New York City (day length of 15:05 h), whereas in Santiago, Chile the sun rose at 7:46 AM and set at 5:42 PM (day length of 9:56 h). For illustrative purposes we will take NYC to have an $N = 15$ h photoperiod with sunrise at 5:30 AM ($x = 0$) and sunset at 8:30 PM ($x = 15$), and Santiago to have an $N = 10$ h photoperiod with sunrise at 8 AM ($x = 0$) and sunset at 6 PM ($x = 10$).

The flight time from New York City to Santiago is roughly 13 h. Consider a leaving time of 10 AM from New York City with an arrival time of 11 PM in Santiago. Let us assume that the traveler is initially entrained to the NYC LD-entrained solution and remains so through the duration of the flight. Thus on arrival in Santiago, the traveler would be expecting 6.5 h of darkness, but instead re-

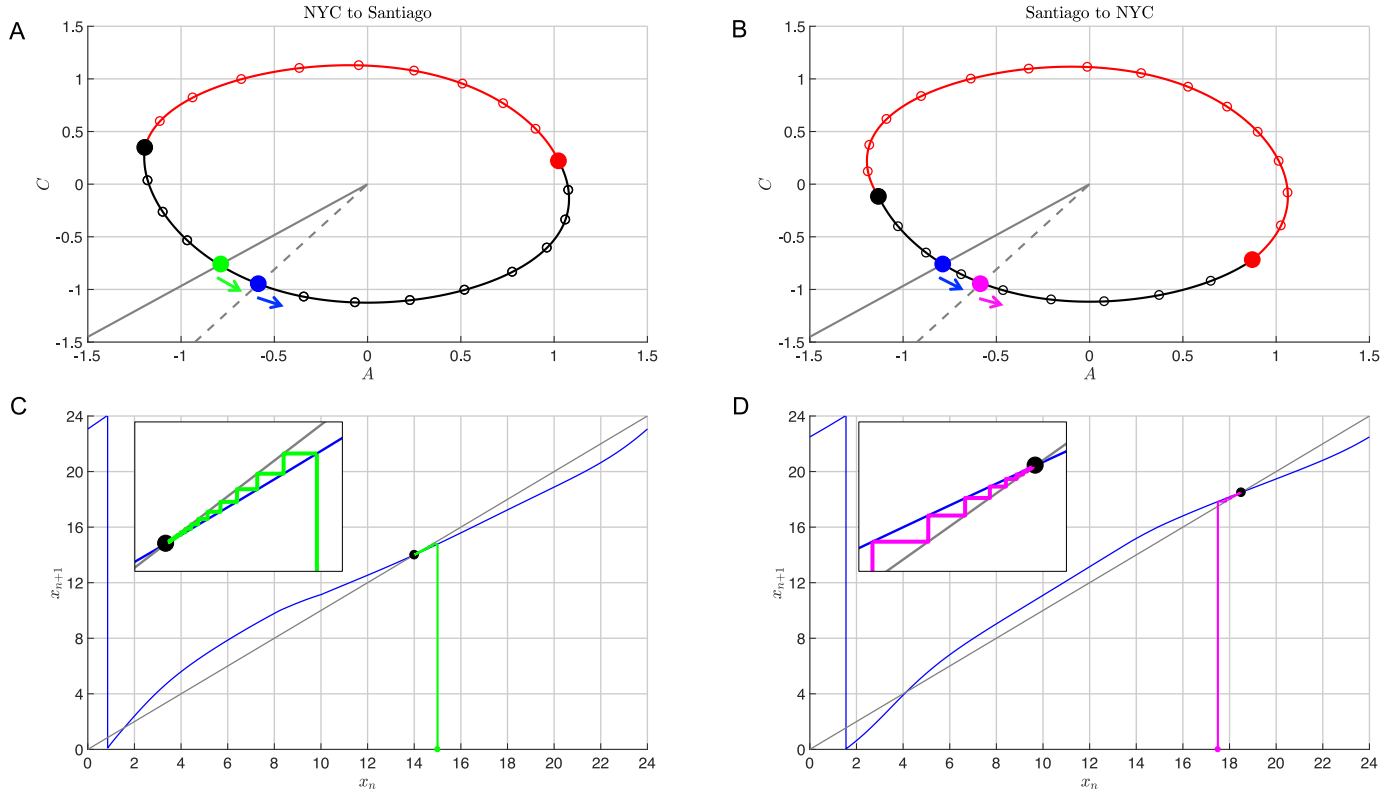

Fig. 13. Change in daylength due to north-south travel can cause jet lag. For all panels, $\tau_c = 24.2$ h and $I = 1000$ lux. (A) LD-entrained solution in Santiago on June solstice (photoperiod $N = 10$ h). The sun rises at 8 AM (red dot) and sets at 6 PM (black dot). The green dot represents a traveler from NYC that arrives in Santiago at 11 PM and is still entrained to the NYC LD cycle, where 11 PM corresponds to the $X_{NY} = 17.5$ section denoted by the solid gray line. The blue dot represents a reference oscillator already entrained to the Santiago LD cycle, where 11 PM corresponds to the $X_{SC} = 15$ section denoted by the dashed gray line. Therefore the traveler must reentrain and does so through phase advancing. (B) LD-entrained solution in NYC on June solstice (photoperiod $N = 15$ h). The sun rises at 5:30 AM (red dot) and sets at 8:30 PM (black dot). The magenta dot represents a traveler from Santiago that arrives in NYC at 11 PM and is still entrained to the Santiago LD cycle, where 11 PM corresponds to the $X_{SC} = 15$ section denoted by the dashed gray line. The blue dot represents a reference oscillator already entrained to the NYC LD cycle, where 11 PM corresponds to the $X_{NY} = 17.5$ section denoted by the solid gray line. Therefore the traveler must reentrain and does so through phase delaying. (C) Entrainment map for NYC to Santiago travel arriving at 11 PM. The stable fixed point is located at $x_s = 14.003$, which is where the $X_{NY} = 17.5$ section (solid gray line) intersects the $N = 10$ LD-entrained solution in (A). The initial condition is located at $x_0 = 15$, because upon arrival the traveler will experience 9 h of darkness before the sun rises. Cobwebbing the map yields reentrainment through phase advance (see inset), in agreement with direct simulation. (D) Entrainment map for Santiago to NYC travel arriving at 11 PM. The stable fixed point is located at $x_s = 18.496$, which is where the $X_{SC} = 15$ section (dashed gray line) intersects the $N = 15$ LD-entrained solution in (B). The initial condition is located at $x_0 = 17.5$, because upon arrival the traveler will experience 6.5 h of darkness before the sun rises. Cobwebbing the map yields reentrainment through phase delay (see inset), in agreement with direct simulation. (For interpretation of the references to colour in this figure legend, the reader is referred to the web version of this article.)

ceives 9 h of darkness since the sun does not rise until 8 AM. Thus at arrival, the traveler is not entrained to the Santiago $N = 10$ LD cycle. For now, consider a traveler with a normal internal clock of $\tau_c = 24.2$ h. At arrival, the traveler lies on the $X_{NY} = 17.5$ Poincaré section of the NYC LD-entrained solution. The intersection of this Poincaré section with the Santiago LD-entrained solution occurs for $X_{SC} = 14.005$. For travel from South to North, if a traveler leaves Santiago at 10 AM ($X_{SC} = 2$) and takes a 13-h flight, then arrival in NYC is at 11 PM which is $X_{SC} = 15$ and $X_{NY} = 18.946$. Panel A of Fig. 13 shows the $N = 10$ Santiago LD-entrained solution and Panel B shows the $N = 15$ NYC LD-entrained solution. In Panel B, the solid gray line is the projection of the Poincaré section onto the NYC LD-entrained solution at arrival corresponding to $X_{NY} = 17.5$. The projection of this same Poincaré section onto the Santiago LD-entrained solution at $X_{SC} = 14.005$ is shown in solid gray in Panel A. Similarly for travel from Santiago to NYC, the dashed gray lines correspond to the projection of the Poincaré section at arrival corresponding to $X_{SC} = 15$ of the Santiago LD-entrained solution and $X_{NY} = 18.946$ of the NYC LD-entrained solution.

The change in the stable entrained phase after north-south travel is already predicted by our earlier results concerning the Arnold onion and those of Schmal et al. (2015). North-south travel is equivalent to moving along a vertical slice of Fig. 4D. Knowing that there is a change in stable phase indicates that there may be an associated time to reentrainment, which we can calculate by cobwebbing the appropriate entrainment map.

We first calculate reentrainment via direct simulation. Since the sun will come up in Santiago at 8 AM, we simulate 9 more hours of darkness starting with an initial condition corresponding to 11 PM on the NYC LD-entrained solution ($X_{NY} = 17.5$) and then begin 10:14 LD cycles. At the same time we also start a reference oscillator with initial conditions corresponding to 11 PM on the Santiago LD-entrained solution ($X_{SC} = 15$) and subject it to the same protocol. We keep track of the times that the trajectories cross the Poincaré section $X_{SC} = 14.005$, and when they cross within 0.5 h of each other we declare the traveler trajectory to be entrained. This procedure gives an entrainment time of 71.458 h (see * in Table 1). Note that travel from NYC to Santiago can be considered as a phase delay in the sense that at arrival at 11 PM, the traveler would expect the lights to turn on at the start of the next NYC-based LD cycle after 6.5 h. Instead the lights turn on at the beginning of the next SC-based LD cycle which occurs after 9 h. Thus the traveler is phase delayed with respect to lights on in the arrival time zone.

To compute entrainment time using the map, we build a $N = 10$ map with the Poincaré section at $X_{SC} = 14.005$ on the Santiago LD-entrained solution. Since arriving at 11 PM means there will be 9 more hours of dark before the 10:14 LD cycle begins, we cobweb the map using an initial condition of $x_0 = 15$. This proce-

Table 1
Reentrainment times for southward and northward travel with $\tau_c = 24.2$ h and $I = 1000$ lux.

	Direct simulation			Entrainment map				
	t	t_{ref}	$t_{ref} - t$	x_n	x_{n+1}	$x_s - x_{n+1}$	$\rho(x_n)$	$\Sigma\rho(x_n)$
NYC to Santiago	23.776	23.005	−0.772	15	14.780	−0.775	23.780	23.779
	47.598	47.005	−0.593	14.780	14.622	−0.617	23.842	47.621
	71.459*	71.005	−0.454	14.622	14.465	−0.460	23.843	71.465**
Santiago to NYC	24.3444	24.9960	0.6516	17.5	17.841	0.655	24.341	24.341
	48.5594*	48.9960	0.4366	17.841	18.040	0.456	24.199	48.540**

dure gives an entrainment time of 71.464 h (see ** in Table 1), which is in close agreement to the direct simulation result. Fig. 13C shows a cobweb diagram of the reentrainment process. The trajectory starts with $x_0 = 15$ and phase advances (moves to the left closer to the start of the LD cycle) towards the stable fixed point at $X_{SC} = 14.005$. Thus in this situation, although the travel from North to South is a phase delay, the reentrainment is antidromic through phase advancement. This is in contrast to the norm for east-west travel for which reentrainment is typically orthodromic, i.e. through phase delays when the travel yields a phase delay, and vice versa for advances. Thus, it is surprising that the "natural" mode of reentrainment for travel from north to south at the June solstice for a traveler with a normal body clock is antidromic.

For travel from south to north, if a traveler leaves Santiago at 10 AM ($X_{SC} = 2$) and takes a 13-h flight, then arrival in NYC is at 11 PM which is $X_{SC} = 15$ and $X_{NY} = 18.946$. Following a similar procedure as above, we simulate 6.5 h of darkness before starting 15:9 LD cycles. Through direct simulation the entrainment time is 48.56 h. Similarly, we build the $X_{NY} = 18.946$, $N = 15$ map and check reentrainment with an initial condition $x_0 = 17.5$. Reentrainment time using the map is found to be 48.54 h. Travel from south to north can be considered a phase advance since the traveler will experience the onset of the next LD cycle sooner in NYC than in SC. But, as noted from Fig. 13D, reentrainment is through phase delay. Thus this reentrainment is also antidromic. As seen from the above results, for $\tau_c = 24.2$ h traveling from photoperiods of $N = 10$ to $N = 15$ h incurs roughly the same reentrainment time (2 to 3 days) as traveling from $N = 15$ to $N = 10$ h.

In Fig. 14A we show reentrainment times calculated from direct simulation for travel between NYC and Santiago for τ_c ranging from 22.6 to 26 h. Note, as τ_c decreases, it takes longer to reentrain after the northbound Santiago to NYC trip than the southbound trip. The opposite is true as τ_c increases. Also observe that there are values of τ_c for which there is no jet lag, e.g. $\tau_c \approx$ 23, 24.7.

As we change τ_c, both the NYC LD-entrained and SC LD-entrained solutions change in shape in phase space. This means that the locations of various Poincaré sections change. For arrival at 11 PM, while this still corresponds to lying on the section $X_{NY} = 17.5$, it means that the X_{SC} section changes. Fig. 14B shows the location of the X_{SC} section as a function of τ_c. It is parabolic shaped. What does not change is the location of the initial condition $x_0 = 15$ from which we check reentrainment time. For any fixed τ_c, the vertical distance between the dashed line at $x_0 = 15$ and the blue curve of section locations, which corresponds to the stable fixed points x_s for the respective maps, indicates the distance over which a trajectory would have to evolve in order to reentrain. Note that the curve of sections intersects $x_0 = 15$ at the values $\tau_c \approx 23$ and 24.7. Thus the distance $|x_0 - x_s| < 0.5$ which means that the trajectory is already entrained. This explains why travel for nearby values of τ_c experience no jet lag. Similarly Fig. 14C shows the location of the X_{NY} section as determined from using the $X_{SC} = 15$ section. This curve is also parabolic shaped, but opens down. It intersects the line of initial conditions at $x_0 = 18$ at $\tau_c \approx$ 23 and 24.7 as well.

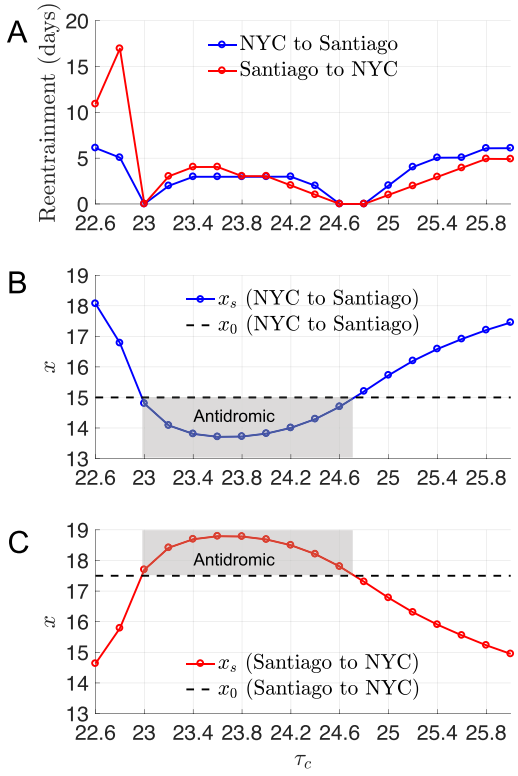

Fig. 14. Reentrainment following north-south travel depends on intrinsic period and is typically antidromic. (A) Jet lag due to north-south travel is most severe for extreme intrinsic periods (greater than 5 days for $\tau_c \le 23$ and $\tau_c \ge 25.4$), with southbound travel (blue) being worse for slow intrinsic clocks and northbound travel (red) being worse for fast intrinsic clocks. (B) Location of stable fixed point x_s and initial condition x_0 for southbound travel as a function of τ_c. Severity of southbound jet lag in (A) reflects the distance between x_s and x_0, with zero days of reentrainment required when x_0 is within 0.5 h of x_s, as is the case for $\tau_c = 23$, 24.6, and 24.8 h. For $23 \le \tau_c \le 24.6$, $x_s < x_0$, therefore reentrainment is through phase advances and is considered antidromic since southbound travel in the month of June is a phase delay of the LD cycle; see text for detailed explanation. (C) Location of stable fixed point x_s and initial condition x_0 for northbound travel as a function of τ_c. Severity of northbound jet lag in (A) reflects the distance between x_s and x_0. For $23 \le \tau_c \le 24.6$, $x_s > x_0$, therefore reentrainment is through phase delays and is considered antidromic since northbound travel in June is a phase advance of the LD cycle. (For interpretation of the references to colour in this figure legend, the reader is referred to the web version of this article.)

For travel from NYC to Santiago, Fig. 14B shows that the curve of sections lies below $x_0 = 15$ for values lying between 23 and 24.7. This means that the stable fixed point lies to the left of the initial condition $x_0 = 15$. Thus reentrainment would occur through advance. However, for τ_c less than 23 or greater than 24.7, the stable fixed point x_s is to the right of $x_0 = 15$ so reentrainment is through phase delay. Since southward travel at the northern solstice is considered to be a delay, this reentrainment can be thought of as being orthodromic. Note that at the extreme values of τ_c, orthodromic reentrainment takes longer than the antidromic reentrainment that occurs for intermediate values $23 < \tau_c < 24.7$. In ad-

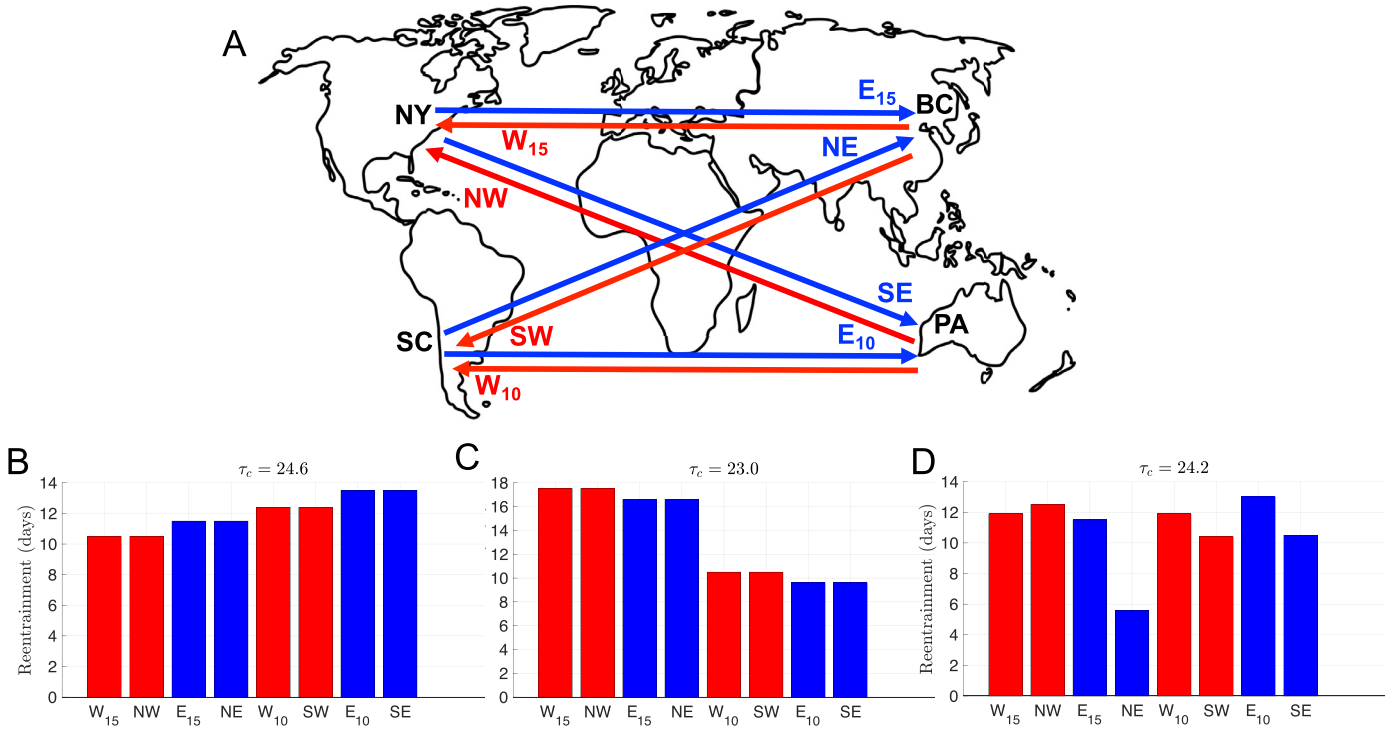

Fig. 15. Jet lag due to trips involving both north-south and east-west travel can be more or less severe than purely eastward or westward travel depending on intrinsic period and daylength. (A) Illustration of trips considered: pure eastward or westward travel between NYC and Beijing (E_{15}/W_{15}) and Santiago and Perth (E_{10}/W_{10}), travel between NYC and Perth (SE/NW), and travel between Santiago and Beijing (NE/SW). NYC and Santiago are 11 time zones away from Beijing and Perth. The trips are made on the June solstice when NYC/Beijing have 15 h of light and Santiago/Perth have 10 h of light. For these simulations we set $I = 1000$ lux. (B) Reentrainment times for $\tau_c = 24.6$ h. For $\tau_c = 24.6$ h, all reentrainment occurs through phase delays. Blue (red) bars correspond to eastward (westward) travel. See text for an explanation of the ordering of reentrainment times. (C) Reentrainment times for $\tau_c = 23.0$ h. In this case all reentrainment occurs through phase advances, and the ordering of reentrainment times is the opposite of the ordering for $\tau_c = 24.6$ h. (D) Reentrainment times for $\tau_c = 24.2$ h. In this case reentrainment can occur either through phase advance (E_{10}), phase delay (W_{15}, NW, W_{10}, SW, and SE), or fast reentrainment through the phaseless set (NE). (For interpretation of the references to colour in this figure legend, the reader is referred to the web version of this article.)

dition, for travel from Santiago to NYC, orthodromic reentrainment for $\tau_c < 23$ takes surprisingly long, on the order of 10 to 15 days. For small τ_c, the $N = 15$ entrainment map is closer to its bifurcation point than the $N = 10$ map. What this means is that the derivative of the map at the stable fixed point x_s is closer to one for the $N = 15$ map compared to the $N = 10$ map. The magnitude of this derivative controls the rate of attraction towards the fixed point. The closer it is to one, the slower the reentrainment. At the other extreme of $\tau_c = 26$ h, the $N = 10$ map is closer to bifurcation. The situation is reversed and southward trips taker longer to reentrain from than northward trips.

3.7. Travel that is both east-west and north-south

Having separately considered jet lag due to east-west and north-south travel, we now consider travel that combines both east-west as well as north-south changes. The main point we would like to address is the extent to which changes in photoperiod synergistically add on to (or subtract from) jet lag due to pure eastward or westward travel. We will consider four different cities, New York City (NY), Santiago, Chile (SC), Beijing, China (BC) and Perth, Australia (PA); see Fig. 15A. The main reason to choose Beijing and Perth is that they lie in the same time zone and have the same photoperiods as New York City and Santiago respectively. We shall assume that on the June solstice, both NYC and Beijing have 15:9 photoperiods with sunrise at 5:30 AM and sunset at 8:30 PM. Santiago and Perth are both under 10:14 photoperiods with sunrise at 8:00 AM and sunset at 6:00 PM. Both Beijing and Perth are 11 time zones east of NYC and Santiago. We assume that the traveler stays entrained to the HTZ during travel. Initially, we will work with two different periods of the intrinsic clock, $\tau_c = 23$ and 24.6 h. We choose these representative values because results from the prior section indicate that strict north-south travel for individuals with these clocks produces no jet lag. Thus an interesting question to explore is whether northeast and southeast (northwest and southwest) travel have different jet lag than pure eastward (pure westward) travel.

Fig. 15A shows the different directions of travel that we shall consider. The directions SE, SW, NE and NW are self-explanatory. The directions E_{10}, W_{10}, E_{15} and W_{15} refer to east-west travel under conditions of $N = 10$ h for travel between Santiago and Perth and $N = 15$ h for travel between NYC and Beijing. Fig. 15B shows reentrainment times for various modes of travel for $\tau_c = 24.6$ h with $I = 1000$ lux. There are effectively four pairs of reentrainment times:

$$W_{15} = NW < E_{15} = NE < W_{10} = SW < E_{10} = SE. \quad (8)$$

Below we shall explain why these pairs exist and why the ordering of reentrainment times follows this pattern. For now, note that SE travel has more jet lag than E_{15}, and SW travel has more jet lag than W_{15}. These results show how the change in photoperiod affects travel over different time zones. Consider the NYC, Beijing, Perth triangle. Travel from NYC to Beijing requires 11 days for reentrainment. Travel from Beijing to Perth requires zero days of reentrainment. Yet travel from NYC to Perth requires 13 days of reentrainment despite the fact that strict north-south travel incurs no jet lag. Fig. 15C shows reentrainment times for $\tau_c = 23.0$ h with $I = 1000$ lux. Here, as would be expected, the ordering of the reentrainment times is exactly the opposite than the larger τ_c case:

$$W_{15} = NW > E_{15} = NE > W_{10} = SW > E_{10} = SE. \quad (9)$$

What is different is the degree to which north-south travel affects jet lag, as illustrated by looking at the same travel triangle as above. Beijing to Perth still requires zero days of entrainment. Now E_{15} travel from NYC to Beijing requires 17 days for reentrainment, while the NYC to Perth travel only requires about 10 days to reentrain.

The reentrainment calculations for SE, SW, NE and NW travel combine the protocols that we had employed earlier to calculate reentrainment due to east-west or north-south travel. In particular, we choose Poincaré sections as for north-south travel, but now adjust the initial condition to take the change in time zone into consideration. For example, consider travel from NYC to Perth with arrival occurring at 10 AM Perth local time (DTZ). This corresponds to 11 PM NYC local time (HTZ). The traveler, by assumption, remains entrained to the NYC LD cycle. Thus at arrival in Perth, the traveler is at $X_{NY} = 17.5$. We compute where this Poincaré section intersects the $N = 10$ Perth LD-entrained solution, which occurs at $X_{PA} = 14.697$ for $\tau_c = 24.6$ h, and $X_{PA} = 14.803$ for $\tau_c = 23.0$ h. We build an entrainment map for the $N = 10$ LD-entrained solution and compute the reentrainment time with initial condition of $x_0 = 2$. We choose this initial condition because arrival at 10 AM in Perth where sunrise occurs at 8AM means that 2 h of light have already occurred. Travel that is SW, NE, or NW is handled analogously.

To understand why certain pairs of travel have the same reentrainment time, consider the result that E_{10} = SE. Above, we have already described the reentrainment protocol for SE travel. Now consider Santiago to Perth with arrival at 10 AM local Perth time (DTZ), which is 11 PM local Santiago time (HTZ). Now this corresponds to $X_{SC} = 15$. Our protocol for east-west travel dictates that we use $X_{PA} = 15$ and again choose $x_0 = 2$. Thus travel to Santiago from Perth (E_{10}) differs from NYC to Perth (SE) only to the extent that the entrainment maps being used are $X_{PA} = 15$ compared to $X_{PA} = 14.697$ (E_{10}) or 14.803 (SE). Both use the same initial condition $x_0 = 2$. Thus the reentrainment time to these two different, but relatively close fixed points is nearly identical. Similar arguments show why the other three pairs of travel have nearly identical reentrainment times.

To explain the ordering of reentrainment times, take the case $\tau_c = 24.6$ h, where we know that eastward travel is worse than westward travel. Thus $W_{10} < E_{10}$ and $W_{15} < E_{15}$. The reason that $E_{15} < W_{10}$ has to do with how far the $N = 15$ and $N = 10$ maps are from bifurcating. As τ_c increases, the fixed points of the $N = 15$ map bifurcate before those of the $N = 10$ map. Thus for $\tau_c = 24.6$ h the $N = 15$ map has a slope that is closer to one at its stable fixed point $x_s = 17.5$ then the $N = 10$ map at its stable fixed point $x_s = 10$. As stated in the previous section, entrainment times increase dramatically when the map is close to bifurcation. When $\tau_c = 23$ h, the $N = 10$ map is closer to bifurcating than the $N = 15$ map and this causes $W_{10} < E_{15}$ for this case. In fact for this case, the closeness of the map to bifurcation explains why the W_{15} reentrainment times are so much longer than the E_{10} times.

The choices of $\tau_c = 23.0$ and 24.6 h were taken because those were the ones at which strict north-south travel incurs no jet lag. The entrainment times for those two cases are anti-symmetric in their ordering. For a normal human traveler with $\tau_c = 24.2$ h, one might expect entrainment times to fall somewhere between those of the two specific cases. However, we would not expect the pairing of certain reentrainment times to continue to exist. Panel D of Fig. 15 confirms, in part, these observations. First, reentrainment times do generally lie between those of the two specific cases for each of the respective trips. Further, there is no pairing of entrainment times for certain trips since the Poincaré sections used to build the pairs, now, need not lie close to one another. We can explain the difference in reentrainment times within these pairs using the maps for north-south travel with $\tau_c = 24.2$ h shown in Fig. 13.

Consider the pair W_{15} and NW, which reentrain according to similarly-shaped maps with $N = 15$ and $x_0 = 6.5$, where $x_s = 17.5$ (18.498) and $x_u = 3.048$ (4.144) for W_{15} (NW). Therefore both travelers reentrain through phase delays, however the NW traveler starts closer to x_u and has to cobweb further to get to x_s than does the W_{15} traveler. Thus the maps predict that NW will take longer to reentrain, which is consistent with the direct simulation results shown in Fig. 15D (12.5 versus 11.9 days).

Next consider the pair W_{10} and SW, which reentrain according to similarly-shaped maps with $N = 10$ and $x_0 = 4$, where $x_s = 15$ (14.003) and $x_u = 2.781$ (1.565) for W_{10} (SW). Again both travelers reentrain through phase delays, however the SW traveler starts further from x_u and does not have to cobweb as far to get to x_s as does the W_{10} traveler. Thus the maps predict that SW will take less time to reentrain, which is consistent with the direct simulation results (10.4 versus 11.9 days).

To summarize, we have found that NW travel incurs worse jet lag than W_{15}, whereas SW travel incurs less jet lag than W_{10}. In both cases the westward component of the travel leads to reentrainment through phase delay. What is different is that in the former case, the northbound component of the travel also requires the traveler to phase delay to reentrain to the shorter photoperiod, while in the latter case the southbound component requires the traveler to phase advance to reentrain to the lengthened photoperiod. For NW the change in time zone and change in photoperiod exacerbate each other leading to longer total reentrainment than pure westward travel in the northern hemisphere. For SW the change in time zone and change in photoperiod counteract each other leading to shorter total reentrainment time than pure westward travel in the southern hemisphere.

Now consider eastward travel, starting with the E_{10} and SE pair. These reentrain according to the $N = 10$ maps with $x_0 = 2$, where x_s and x_u are the same as for W_{10} and SW. Here the maps predict that the Santiago to Perth traveler reentrains through phase advances, but the NYC to Perth traveler reentrains through phase delays. Thus the change in photoperiod encountered by the SE traveler has moved the unstable fixed point enough that the southbound component of the travel reverses the direction of reentrainment with respect to pure eastward travel. Since the two travelers reentrain in different directions and thereby traverse different x values of the map, it is difficult to say which one will reentrain faster based solely on knowledge of the locations of x_s and x_u. However cobwebbing the map predicts that E_{10} reentrainment time will be longer than SE. These predictions regarding reentrainment times and directions are confirmed by the direct simulation results (13.0 days for E_{10} versus 10.5 days for SE).

Finally, consider the E_{15} and NE pair. These reentrain according to the $N = 15$ maps with $x_0 = 4.5$, where x_s and x_u are the same as for W_{15} and NW. Both travelers reentrain through phase delays, with the NE traveler starting closer to x_u and having to cobweb further to get to x_s than the E_{15} traveler. Thus the map predicts that NE will take longer to reentrain, however this is not what we find in direct simulation. Instead, the Santiago to Beijing traveler reentrains much more quickly (5.6 days) than the NYC to Beijing traveler (11.5 days), as shown in Fig. 15D. The reentrainment time for NE is shorter than predicted by the map due to the initial condition $x_0 = 4.5$ being very close to $x_u = 4.144$ and hence in the phaseless set of the NE map. As discussed in Section 3.5, with the higher intensity light level used for these simulations ($I = 1000$ lux), reentrainment times for initial conditions lying in the phaseless set can be dramatically short.

4. Discussion

For this study of jet lag, we chose the FJK model because it has been fit to human data on how light affects the circadian system (Forger et al., 1999; Jewett and Kronauer, 1998; Kronauer, 1990; Kronauer et al., 1999), has been extensively validated through experiments (Van Dongen, 2004), and has been used in "real-world" applications such as fatigue and performance modeling (Dean et al., 2007). Previous work employing the FJK model in the context of jet lag includes (Dean et al., 2009; Qiao et al., 2017; Serkh and Forger, 2014; Zhang et al., 2016), all of which used techniques from optimization or control theory to design light exposure schedules for the traveler to follow after reaching their destination in order to minimize reentrainment time. In our study, we assumed that the traveler will experience light according to the natural LD cycle in the destination and do not attempt to design alternative light exposure schedules. Instead, we systematically characterized how reentrainment depends on parameters such as the period of the endogenous circadian oscillator, the photoperiod and light intensity of the external LD forcing, the number of time zones crossed, the direction of travel, and the time of day at which the trip occurs.

The main mathematical tool that we used in this paper is the construction and analysis of a set of entrainment maps. These maps determine how the phase of light onset changes each time a trajectory passes through a prescribed Poincaré section of the phase space. Entrainment map analysis offers several advantages. First, the maps depend on parameters in predictable ways that yield important findings on how the dynamics of the full set of equations actually evolve. For example, we showed here how the maps depend on endogenous period τ_c, photoperiod N, and light intensity I. The parameter dependence was qualitatively similar to what we had found in an earlier study (Diekman and Bose, 2016) of circadian models (Gonze et al., 2005; Kim and Forger, 2012; Tyson et al., 1999), indicating that the map is capturing generic properties of circadian oscillators. Next, the fixed points of the entrainment map provide valuable information about the reasons for the underlying dynamics of circadian models. For example, when the map is constructed from a numerically obtained LD-entrained solution, then the stable fixed point of the map x_s corresponds to this stable limit cycle. The stability of x_s is easily determined by visual inspection of the slope of the map at x_s. The unstable fixed point of the map, x_u, can correspond to an actual unstable orbit of the system, but, as demonstrated here, this is dependent on other factors such as the light intensity. However, the unstable fixed point definitely provides evidence for a location in phase space where trajectories either reentrain through phase advance or delay. For instance, we located Z_D, a demarcation point, along the LD-entrained solution using information from x_u. Perhaps the biggest advantage of the map is that it simultaneously provides information about both the stable and unstable phases, as well as the time it takes initial conditions to converge to the stable phase through the cobweb procedure. This is in contrast to methods based on phase response curves or Arnold tongues/onions, which primarily give information about the stable phase but not the dynamics of the reentrainment process.

We used a combination of direct simulations and entrainment map analysis to obtain our results. In many cases, the map was used to organize and explain mathematically the results and observations obtained through direct simulations. Whereas in other cases, analysis of the map provided information that simulations alone would not likely have found. While discussed in more detail below, we would like to emphasize that the map was particularly helpful in identifying certain mathematical objects that play a key role in the FJK model. First, the map was used to find the existence of neutral period curves for different length trips. Using the first iterate of the map as a proxy for reentrainment times, we defined a neutral period point as an east or west trip for which the distance of the map from the diagonal is the same. This allowed us to explain the existence of the east-west asymmetry of jet lag. Next, the map explained which circumstances led to antidromic versus orthodromic reentrainment. Finally, the map revealed the existence of unstable periodic solutions for low light intensity. This led us to better understand the phase space structure of the full FJK model for all lux levels and to speculate about what geometric structure provides a separatrix-like effect for phase advancing versus phase delaying trajectories. Both of these latter two findings are related to the unstable fixed point of the map, which we discuss in more detail in the Appendix.

4.1. Neutral period and east-west asymmetry

Many travelers experience more severe symptoms of jet lag after traveling east than they do after traveling west (Sack, 2009; Waterhouse et al., 2007). The typical explanation for this asymmetry is that since the endogenous period of the human circadian clock is greater than 24 h, it is easier to phase delay the clock and entrain to the phase delay of sunrise/sunset that occurs following westward travel than it is to phase advance the clock and entrain to the phase advance of sunrise/sunset that occurs following eastward travel (Eastman and Burgess, 2009; Monk et al., 2000). Our analysis agrees with this explanation in general but adds an important distinction: while the directional asymmetry does depend on endogenous period, we find however that whether the endogenous period is greater than or less than 24 h is not the critical factor. Instead, we suggest it is a generic property of circadian limit cycle oscillators that there exists a "neutral" endogenous period for which equivalent advances or delays of the LD cycle (i.e. eastward or westward travel across the same number of time zones) will induce the same amount of jet lag. Clocks with an endogenous period greater than the neutral period suffer worse jet lag after eastward travel and those with an endogenous period less than the neutral period suffer worse jet lag after westward travel. The neutral period terminology was introduced by Aschoff et al. (1975), who studied the asymmetry effect in a variety of species and a mathematical model (Wever, 1966). We find that the neutral period depends on daylength and, as a result, we generalize this notion to a neutral period curve (see Figs. 10 and 11). For example, considering east/west trips of 6 time zones and $I = 100$ lux, we found the neutral period to be 24.2 under long days (15:9 photoperiod), 24 h for intermediate length days (11:13 photoperiod) and 23.9 under short days (10:14 photoperiod). Thus for a traveler with an endogenous period of 24.1 h, we predict that traveling east will be harder than west in the winter, but that traveling west will be harder than east in the summer, since for $I = 100$ lux these two cases correspond to parameter pairs that lie on opposite sides of the neutral period curve. While the existence of neutral period curves does not depend on light intensity, the shape of the NPC may be dependent on light intensity since a higher lux level increases the concavity of entrainment maps and leads to faster reentrainment. In turn, this may lead to different light intensity-dependent predictions regarding seasonal effects on the difficulty of travel.

In work related to the east-west asymmetry of jet lag, Lu et al. (2016) studied a macroscopic reduction of a globally coupled network of phase models. Their approach is to derive an ordinary differential equation for a complex-valued order parameter that governs whether or not the system is in an entrained or unentrained state. In their model, depending on parameters, this differential equation can have stable and unstable fixed points as well as limit cycle solutions. Lu et al. find that when the endogenous period is larger than 24 h, eastward trips take longer to reentrain

from then westward ones across the same number of timezones. They find the opposite to hold when the endogenous period is less than 24 h. In some sense, their model utilizes 24 h as a neutral period, independent of daylength.

4.2. Threshold separating orthodromic and antidromic reentrainment

After a small phase shift of the LD cycle a circadian oscillator will reentrain orthodromically, i.e. in the same direction as the shift. This corresponds to reentrainment through phase advances after short eastward trips and through phase delays after short westward trips. Longer transmeridian trips that constitute larger phase shifts of the LD cycle and can lead to antidromic reentrainment where travelers reentrain through phase delays after eastward travel or phase advances after westward travel (Arendt et al., 1987; Burgess et al., 2003; Klein and Wegmann, 1977; Takahashi et al., 2001). In a simulation study of a mammalian molecular clock model, Leloup and Goldbeter (2013) found a sharp threshold in the magnitude of the LD phase shift that separates orthodromic and antidromic reentrainment. They showed that phase shifts that put the traveler in the vicinity of this threshold result in very long reentrainment times, similiar to what we find in the FJK model for lux levels corresponding to indoor light. Leloup and Goldbeter used phase response curve (PRC) analysis to roughly predict the location of this threshold, but stressed that using the PRC for this purpose is not straightforward and not very accurate. We have shown that the entrainment map, in particular the unstable fixed point of the map, provides an easy and accurate method of predicting the critical phase shift (or trip) that separates these two modes of reentrainment. Lu et al. (2016) find circumstances where the stable manifold of an unstable saddle fixed point determines whether solutions reentrain through phase advance or phase delay. The authors show this saddle fixed point merges with another fixed point as a parameter is varied. Interestingly, even after the bifurcation, the effect of the saddle is still present in separating phase advance versus phase delay. This is similar to what we find with the increase in the lux level ($I = 100$ increasing to $I = 1000$) causing the unstable fixed point of our map to no longer correspond to an actual unstable periodic orbit. Still, as demonstrated, we find that x_u separates out phase advancing versus phase delaying initial conditions even at high lux.

4.3. Aiming to enter the phaseless set as a strategy for minimizing jet lag

Our results show that as the light intensity is increased, reentrainment times decrease. This is consistent with previous simulation studies of the FJK model (Serkh and Forger, 2014). Moreover, we have shown that the FJK model exhibits the curious phenomenon of very fast entrainment for certain trajectories that pass through the phaseless set when the light intensity is large. For example, for travelers with an endogenous period of 24.2, trips that are roughly 10.5 h to the east place the traveler in a neighborhood of the unstable fixed point of the map. For low lux $I = 100$, this is the worst trip as this leads to the longest reentrainment time (roughly 25 days) compared to all other trips independent of arrival time; see Fig. 8. But once the lux is increased to 1000, the reentrainment time for this same trip is much shorter (on the order of 5 days) due to the "shortcut" that the trajectory takes through phase space; see Fig. 12. However, this seems to depend to some extent on arrival time, e.g. arriving at $X = 2$ instead of $X = 6$ will result in about 10 days of reentrainment. Thus our results suggest that a traveler may actually wish to intentionally make this "worst" trip, provided that the traveler can guarantee exposure to high lux levels during the reentrainment process and the correct arrival time.

Fast reentrainment through the phaseless set is characterized by a suppression of oscillation amplitude where the trajectory enters what is effectively a region of phases that converge at a phase singularity or pinwheel, a manifestation of the phaseless set. When the trajectory enters this pinwheel region, it has a chance of emerging with a phase that is much closer to the entrained phase than when it enters, thereby shortening the reentrainment time. When computing optimal light exposure schedules to reentrain the FJK model in minimum time, Serkh and Forger (2014) found several examples of optimal reentrainment that involved taking a shortcut across the limit cycle and reduction of oscillator amplitude in the middle of the schedule. Consistent with our results, Serkh and Forger only observed this phenomenon at high lux values. In Lu et al. (2016), there is a local minimum of reentrainment times exactly in a neighborhood of the "worst" trip. Though not discussed in their paper, this faster than expected reentrainment may also be related to trajectories taking shortcuts in phase space.

4.4. Jet lag due to north-south travel

The medical definition of jet lag—insomnia, excessive daytime sleepiness, or general malaise associated with transmeridian travel of at least two time zones—precludes the possibility of jet lag due to purely north-south travel (Sack, 2009). Indeed it has been explicitly stated that travel along the same meridian, for example Europe to southern Africa, causes no jet lag (Herxheimer and Waterhouse, 2003). However if one considers a broader definition, such as jet lag symptoms resulting from any travel that shifts the alignment of 24-h environmental cycles relative to the endogenous circadian clock (Song et al., 2017), then it seems plausible that the change in daylength encountered after long-distance translatitudinal travel in the summer or winter could induce jet lag-like effects. In our simulations of the FJK model, we find that it takes about 3 days for an oscillator with the average human endogenous period (24.2 h) to reentrain following travel from summer days with 15 h of light to winter days with 10 h of light, or vice versa. For circadian oscillators with long or short endogenous periods, the reentrainment time following such travel can be a week or more. We used the entrainment map to provide an explanation for these results by showing how the phase of entrainment (the stable fixed point of the map) is affected by daylength. The map and simulations also predict that the natural mode of reentrainment is antidromic, in that traveling from summer to winter constitutes a phase delay of the LD cycle but reentrainment occurs through phase advances. We are not aware of any field, laboratory, or computational studies that have thoroughly explored the question of reentrainment after translatitudinal travel. A review of jet lag by Waterhouse et al. (2007) notes that travel between hemispheres produces disorientation because of changes in natural lighting but does not elaborate further. In a field study with four human subjects, Hauty and Adams (1965a; 1965b; 1965c) included a north to south flight (from Washington, D.C. to Santiago, Chile) as a control to compare against east to west (Oklahoma City to Manila) and west to east (Oklahoma City to Rome) flights, in order to assess the effects solely attributable to a long flight versus effects due to changes in time zone. They found that all three flights produced a significant amount of subjective fatigue, but that the north-south flight did not cause a phase shift of circadian rhythms in physiological measurements such as rectal temperature and heart rate, whereas the other two flights did. However, the time of year that these flights took place is not reported in this study, and so it is possible that the flights were in spring or fall when the daylengths in D.C. and Santiago are similar. Moreover, the endogenous circadian period of the subjects was not reported, so it is difficult to compare their results to our predictions based on the FJK model.

Horses are the only species other than humans that are flown around the world for athletic competitions. The effect on equine physiology and performance of shifts in the LD cycle equivalent to travel across time zones has been assessed using thoroughbred racehorses kept in light-controlled stables (Tortonese et al., 2011). These studies found that horses are highly sensitive to light cues and rapidly adapt to phase shifts in the LD cycle. Surprisingly, athletic performance as measured by treadmill tests was actually enhanced following phase advances of the LD cycle simulating eastward travel. This enhancement was not attributed to an endogenous rhythm in athletic ability, but rather to masking effects of light and a timely rise in the hormone prolactin. In a commentary, the authors of this study note that horses have weak endogenous circadian rhythms but strong circannual biological rhythms (Tortonese and Short, 2012). The robust circannual clock may lead to slow adaptation in response to sudden changes in latitude, in contrast to the fast adaptation seen in response to simulated changes in longitude. Consistent with this prediction, racehorses subjected to simulated transequatorial flights exhibit negative effects on athletic performance (Domingo Tortonese, personal communication).

In our simulations of north-south travel, we have taken the photoperiod to be greater in the northern location ($N = 15$ h) than the southern location ($N = 10$ h) based on the duration of sunlight in the natural light-dark cycles at these latitudes at the selected time of year (June). However, the prevalence of electric lighting in modern society renders the duration of light that the circadian system is exposed to less dependent on the photoperiod of the natural light-dark cycle than it would be in the absence of artificial lighting (Skeldon et al., 2017). Despite the ability to control certain aspects of our light environment, there is still seasonal variation in the amount of light humans are exposed to in industrialized societies, with greater light exposure in the summer months than the winter months (Park et al., 2007). Furthermore, Thorne et al. (2009) found a seasonal effect on the time course of light exposure throughout the day. During the evening hours (5 PM–9 PM in their study), subjects were exposed to significantly more blue light in summer than in winter. Blue light is known to have a more potent phase shifting effect on the circadian clock than light at other wavelengths (Warman et al., 2003), and most artificial light sources contain less blue than natural light. Taken together, these observations suggest that modern humans are exposed to a longer duration of natural light in the summer, and therefore suddenly shifting from summer to winter (for example by traveling from NYC to Santiago in June) may reasonably be modeled as a reduction in N. Nevertheless, extensions of the entrainment map methodology to handle more realistic self-selected light exposure patterns would be useful for making quantitative predictions about the extent of north-south jet lag.

4.5. Traveling diplomat problem

The idea of minimizing reentrainment times has relevance for what we shall call the traveling diplomat problem. For example, the three most recent U.S. Secretaries of State traveled extensively during their tenures. John Kerry covered more than 1.3 million miles, Hillary Clinton visited 112 countries, and Condoleeza Rice made a total of 241 visits to foreign countries, all records within those categories (Chow and Kessler, 2013; Kelemen, 2016). The problem one can consider is analogous to a traveling salesman problem in which the salesman has to arrange travel to several locations so as to minimize total travel distance. In our scenario, a diplomat would seek to arrange his/her schedule to minimize jet lag. If a diplomat wished to visit a certain number of countries in the span of a certain number of days before returning home, could she arrange her travel to minimize her jet lag in each of the destination cities and also upon return home? Or if she were to remain in each destination city until reentrained, before continuing to the next city, does an optimal path exist that minimizes total jet lag? Our results suggest that the diplomat could arrange her travel path to minimize jet lag. For example assuming a normal endogenous period of 24.2 h, if the diplomat were to travel between the four cities we studied, she would want to incorporate a NE component of travel; see Fig. 15. The loop NYC → Santiago → Beijing → Perth → NYC would cause her to have the least overall amount of jet lag. Santiago to Perth has 12 days of reentrainment, and Perth to Beijing 2 days, for a total of 14 days of reentrainmnent. But Santiago to Beijing has 5 days and Beijing to Perth 3 days, for a total of only 8 days of reentrainment. Thus by specifically including the NE component in her itinerary, she would minimize jet lag. The total number of reentrainment days for the NYC → Santiago → Beijing → Perth → NYC is 23 days. Another loop that has a relatively short reentrainment time is NYC → Perth → Beijing → Santiago → NYC which has 24 days of reentrainment. This loop has the advantage of two direct northward trips compared to the previous loop of two direct southward trips. This saves 2 days. Also, SE travel compared to NW travel saves 2 days. It is only because SW travel requires 5 more days of entrainment than NE that this loop is slightly worse than the previous. In comparison the loops NYC → Santiago → Perth → Beijing → NYC or NYC → Beijing → Perth → Santiago → NYC each lead to 28 days of jet lag. The example presented here is for a single daytime lux level, which is surely a simplification of what a diplomat or other traveler would likely experience. In reality, travelers would experience a variety of lux levels across their waking hours dependent on being exposed to indoor or outdoor light. As noted in our earlier results, higher lux levels lead to faster reentrainment but do not significantly affect the phase of the entrained solution. Thus we expect that even when a traveler experiences a more realistic light protocol than the single lux scenario presented here, there would still exist travel paths that minimize jetlag.

4.6. Future directions

There are several directions of further research that can be pursued. We plan to explore the effects of “social jet lag” where individuals stay up late on weekend nights, sleep in later the next day, and then return to their normal schedules for the work week (Crowley and Carskadon, 2010). This can be likened to taking a trip two or three hours west on a Friday night and returning home on Sunday night. Presumably, individuals who do this for several weeks in a row are not entrained to the daily light-dark cycle, but instead entrain to a more complicated weekly pattern (Smith and Eastman, 2012). Using the methods developed in this paper, we could study this problem by looking for a periodic solution, rather than a fixed point, of a set of composed entrainment maps. The added complication of using multiple maps arises as one must take into consideration the change of photoperiod that would occur due to staying up late and waking up late. We also plan to apply our methods to analyze night-shift work, which also involves periodic solutions of composed entrainment maps due to different light exposure and sleep schedules on weekdays versus weekends. Another situation where a periodic solution of the entrainment map would be relevant is for individuals who, because their endogenous period is too far from 24 h, are unable to entrain to LD forcing (Duffy and Wright, 2005). In all of these cases, the goal of our research would be to first find a stable periodic orbit of the entrainment map, and then find strategies (perturbations, perhaps of the light exposure) to move the individual closer to an entrained state.

The light-dark cycle is not the only external forcing that a circadian oscillator receives. For example, the effects of meals, exer-

cise, or taking melatonin can also be considered as external stimuli. We would like to generalize the entrainment map to incorporate multiple zeitgebers of this type. The main question to address is how a weaker, and perhaps conflicting, forcing signal would interact with the stronger light-dark forcing to determine entrainment properties. Another factor to consider is the entrainment of peripheral oscillators in tissues throughout the body by the suprachiasmatic nucleus (SCN), the master circadian pacemaker located in the hypothalamus. During jet lag, there can be internal desynchrony due to the SCN and peripheral oscillators reentraining at different rates or even in opposite directions, a phenomenon known as reentrainment by partition (Aschoff, 1978). Leise and Siegelmann (2006) studied reentrainment of a multistage computational model of the circadian system. Our approach would be to construct entrainment maps for each system component with some form of coupling among the maps. There is also significant coupling between the SCN and sleep-wake control centers in the brain (Vosko et al., 2010). Jet lag can desynchronize the circadian rhythm of the SCN and sleep-wake behavior. Models combining the circadian pacemaker and sleep-wake dynamics have been proposed (Gleit et al., 2013; Phillips et al., 2010; Skeldon et al., 2015), and one-dimensional maps for the circadian modulation of sleep have been developed (Booth et al., 2017; Nakao et al., 1997; Skeldon et al., 2014). An important future direction is to investigate the relationship between these maps and entrainment maps in the context of jet lag and other circadian rhythm sleep disorders.

Acknowledgments

We thank Somini Sengupta for helpful feedback regarding the traveling diplomat problem. This material is based upon work supported in part by the National Science Foundation [grant numbers DMS-1412877, DMS-1555237], and the U.S. Army Research Laboratory and the U.S. Army Research Office [contract/grant number W911NF-16-1-0584].

Appendix

In this Appendix, we further discuss the relationship between the fixed points x_s and x_u of an entrainment map and the dynamics of the forced FJK model. Given that we have considered many different entrainment maps, let us focus on the map constructed by taking a Poincaré section at $X = 6$ along the LD-entrained solution obtained for $\tau_c = 24.2$ h and $N = 12$ h. To construct the map, we choose initial conditions for A, C, and n that lie at the intersection of the Poincaré section and the LD-entrained solution and vary the value of the offset of the lights x between 0 and 24. The value $x_s = 6$ of the map therefore will correspond exactly to a periodic orbit of the FJK model because the trajectory returns to $X = 6$ after exactly 24 h and for this case the A, C, and n values return to their original values after 24 h. In general, when the entrainment map is constructed using a Poincaré section that intersects an LD-entrained solution and A, C, and n initial conditions at that intersection point, there is a direct correspondence between x_s and the stable LD-entrained solution.

The relationship of x_u to dynamic structures of the forced FJK model is more complicated. On one hand, we have found that the existence of a corresponding unstable periodic orbit depends on light intensity I. On the other hand, we have found that independent of light intensity, x_u corresponds to a structure in phase space that separates trajectories that phase advance or phase delay as they converge to the entrained solution. We explain both of these observations below.

First, consider low light intensity of $I = 100$ lux. For this case, $x_u = 16.24$. This means that the demarcation point predicted by our map is a journey given by $Z_D = 10.24$ time zones to the east. In Fig. 16A, the projection of the stable LD-entrained solution onto the $A - C$ plane is plotted in solid red and black. The location $Z = 0$ and $X = 6$ (solid blue circle) coincide. The projection of the unstable periodic orbit is plotted in dashed red and black. Travel east corresponds to moving clockwise along the projection of the stable orbit to a location marked by an open blue circle on the LD-entrained solution. In terms of x, this value is called $\hat{x}_u = x_s - Z_D$ mod 24 and equals $x = 19.8$. The map predicts that this location along the LD-entrained solution separates trajectories that converge via phase delay or advance. Note that this interpretation is equivalent to the one given in Section 3.5 where the trajectory began on the Poincaré section with different light offset initial conditions taken in a neighborhood of x_u. Here we instead fix the light offset to be $x = 6$ and vary the initial conditions in a neighborhood of $\hat{x}_u$ chosen by making a trip Z_D time zones on the LD-entrained solution. Panel A shows a stroboscopic map (solid dots) of different initial conditions projected onto the $A - C$ plane every 24 h. From each initial condition, we ran a simulation under 6 h of light, followed by 12 h of dark, and then 6 h of light before plotting the ensuing location of the trajectories, and then repeated. From just to the left of $\hat{x}_u$ emanates a set of points, also in dark blue, that converge towards a point corresponding to $X = 6$ on the unstable periodic orbit. Thus these points lie on the *stable* manifold of the unstable periodic orbit! Finding this manifold without the insights provided by the entrainment map would have been extremely unlikely. The unstable periodic orbit appears to be a saddle with a stable manifold that is at least 2-dimensional. The saddle-like nature makes backward integration largely useless in locating the unstable periodic orbit. Instead it is the entrainment map that provided the clue on where to locate it in the full phase space. The initial conditions at $Z = 10$ and $Z = 11$ start on "opposite sides" of the stable manifold of the unstable orbit and are seen to produce a sequence of iterates that converge to $X = 6$ on the stable periodic orbit by phase advancing (green) or delaying (magenta); see Fig. 16B. In another set of simulations, we chose initial conditions very close to the solid blue separatrix on the LD-entrained solution and these also entrained by advance or delay depending on from which side of the stable manifold they originated (data not shown). Finally, observe the cyan set of dots that emanate from $X = 6$ on the unstable orbit and then converge to the stable LD-entrained solution at $X = 6$. The initial cyan dot that we chose as an initial condition was found in the following way. We located the value of (A^*, C^*, n^*) at which the unstable periodic orbit intersected the Poincaré section at $X = 6$ on the unstable orbit. We then perturbed the A and C values to $A^* - 0.00271035$ and $C^* + 0.01$, but kept $n = n^*$. Therefore after 24 h the n value returns to n^*. Thus all the cyan dots lie in the plane $n = n^*$. These points are seen in both Fig. 16A and B to take a shortcut across (through) phase space towards the stable LD-entrained solution. The trajectory is characterized by the fact that it neither phase advances or delays for the first few iterates until it undergoes amplitude suppression. After it reemerges to full amplitude it effectively has the correct phase of the LD-entrained solution. We suspect that these points lie on the strong stable manifold of the stable LD-entrained solution. We speculate that this strong stable manifold separates phase advancing or phase delaying trajectories, in general, independent of the light intensity I. The figure also shows points that initially lie close to the cyan points but then follow the more predictable advance (green) or delay (magenta).

Now consider Fig. 16C and D which show the corresponding plots for a higher light intensity of $I = 1000$ lux. For this case, $x_s = 6$ remains, but now $x_u = 16.68$. Thus the demarcation point is $Z_D = 10.68$ or $\hat{x}_u = 19.32$. Panel C shows the projection onto the $A - C$ plane and Panel D shows a few representative sequences of iterates in the three-dimensional phase space. The main difference to note is there is no unstable periodic orbit. Instead the sequence

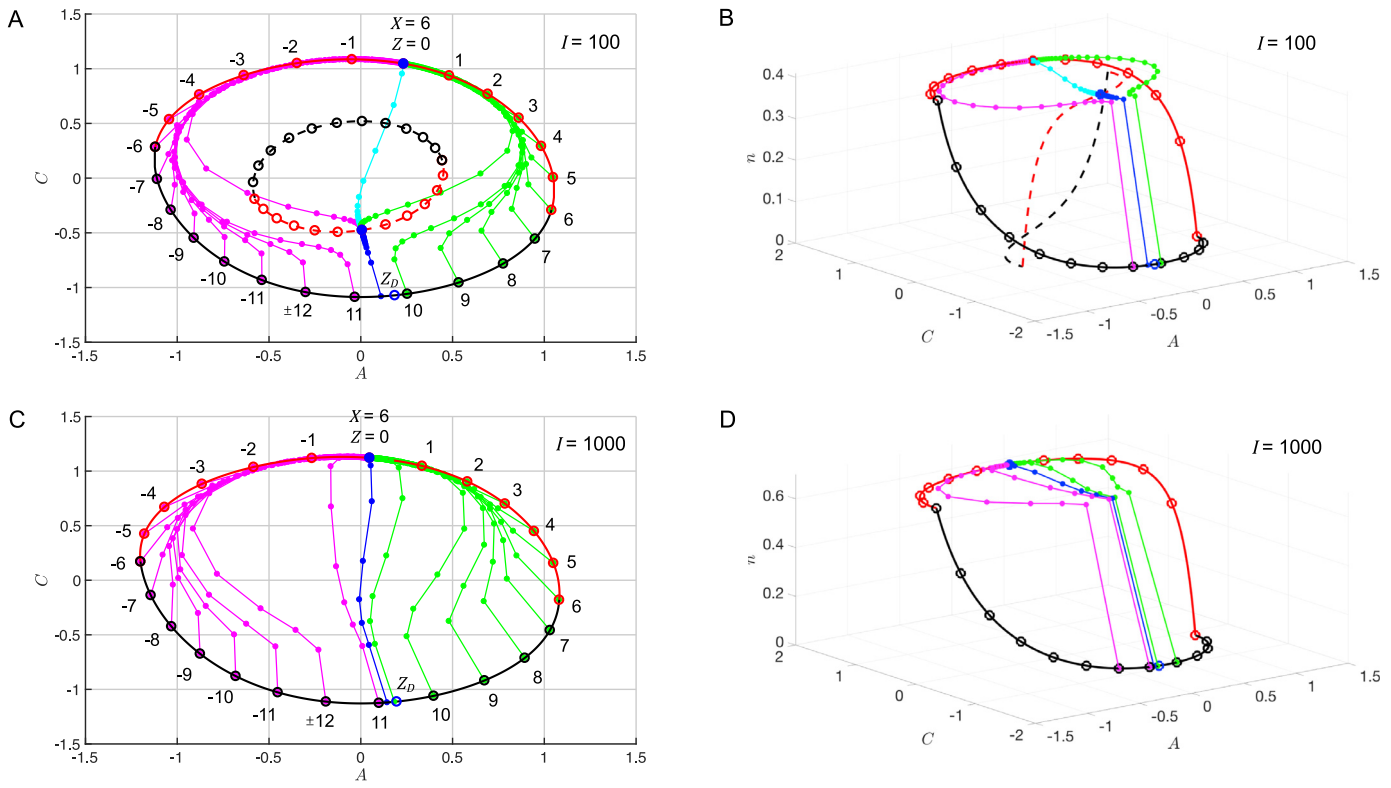

Fig. 16. Relationship between the unstable fixed point of entrainment map and dynamics of the FJK model. (A) Projection of stable LD-entrained solution (solid red/black lines) onto $A-C$ phase plane for $\tau_c = 24.2$ h, $N = 12$ h, and $I = 100$ lux. Simulations were performed starting from initial conditions on the LD-entrained solution at the hourly markings denoted by the open red and black circles with a light-dark protocol based on $x = 6$. Positions labeled with $Z > 0$ ($Z < 0$) correspond to travel Z time zones to the east (west). The reentrainment process is depicted by strobing the system every 24 h and plotting the location of the trajectory (solid green and magenta dots). These trajectories converge to $X = 6$ (solid blue circle) by either phase advance (green) or phase delay (magenta). The blue set of dots emanating from near the open blue circle ($Z_D = 10.24$) does not phase advance or delay, and and converges to $x = 6$ on the unstable LD-entrained solution (dashed red and black lines, open circles red and black circles are hourly markings). These points lie on the stable manifold of the unstable periodic orbit, which serves to separate trajectories that entrain through phase advance and delay. The cyan dots are on a trajectory that starts near the unstable periodic orbit and takes a shortcut to converge to $X = 6$ on the stable LD-entrained solution, whereas nearby initial conditions converge to $X = 6$ by phase advancing or delaying. (B) Same objects as Panel A, plotted in the three-dimensional phase space A, C, n. (C) Projection of stable LD-entrained solution (solid red/black lines) onto $A-C$ phase plane for $\tau_c = 24.2$ h, $N = 12$ h, and $I = 1000$ lux. Unlike Panel A, here there is no unstable LD-entrained solution. The blue dots emanating from near $Z_D = 10.68$ are on a shortcut trajectory that exhibits amplitude suppression and converges to $X = 6$ unusually fast. Trajectories on either side of the blue trajectory converge to $X = 6$ through phase advance (green) or delay (magenta). (D) Same objects as Panel C, plotted in the three-dimensional phase space A, C, n. (For interpretation of the references to color in this figure legend, the reader is referred to the web version of this article.)

of dark blue dots that emanate from near Z_D converge directly to the stable LD-entrained solution at $X = 6$. The corresponding sequence behaves in the same way as the cyan sequence of Panel A. Nearby initial conditions also lead to a sequence of iterates that behave quite similarly to the blue one, which is in contrast to the $I = 100$ lux case. What we believe to be common between the two cases is that there exists a structure in phase space, perhaps the strong stable manifold associated with the point on the LD-entrained solution at $X = 6$, that separates phase advancing and phase delaying trajectories. What differs between the two cases appears to be that the shortcut is only accessible from the LD-entrained solution when an unstable periodic orbit does not exist. When it does, the stable manifold of the unstable periodic orbit appears to preclude the possibility of taking the shortcut and accessing the phaseless set. In summary, the entrainment map, and in particular, the unstable fixed point x_u and its corresponding demarcation point Z_D, provide a way to locate specific subspaces within the larger phase space that help organize the dynamics.

Finally, let us address the quantitative difference in the worst case travel between the map and direct simulation shown in Fig. 8D for $\tau_c = 23.4$ h, $I = 100$ lux. For this set of parameters, an unstable periodic orbit exists similar to the one shown in Fig. 16A and B. We believe that in direct simulation, the worst case travel $Z = -6$ is placing the trajectory very close to the stable manifold of the unstable orbit. In turn, this causes the entrainment time to increase. We don't fully understand why the demarcation point Z_D predicted from the map is further from the actual demarcation value from the simulation for $\tau_c = 23.4$ h than it is for the other τ_c values shown in Fig. 8A–C. We believe, however, that is related to the fact that the system (and entrainment map) are closer to bifurcation for this τ_c value (see Fig. 9D) than it is for the others, and thus the unstable and stable limit cycles are quite close to one another in phase space.

References

Arendt, J., Aldous, M., English, J., Marks, V., Arendt, J., Folkard, S., 1987. Some effects of jet lag and their alleviation by melatonin. Ergonomics 30, 1379–1393.

Aschoff, J., 1978. Problems of re-entrainment of circadian rhythms: asymmetry effect, dissociation and partition. In: Environmental Endocrinology. Springer, pp. 185–195.

Aschoff, J., Hoffmann, K., Wever, R., 1975. Re-entrainment of circadian rhythms after phase shifts of the zeitgeber. Chronobiologia 2, 23–78.

Booth, V., Xique, I., Diniz Behn, C., 2017. A one-dimensional map for the circadian modulation of sleep in a sleep-wake regulatory network model for human sleep. SIAM J. Appl. Dyn. Syst. 16 (2), 1089–1112.

Bordyugov, G., Abraham, U., Granada, A., Rose, P., Imkeller, K., Kramer, A., et al., 2015. Tuning the phase of circadian entrainment. J. R. Soc. Interface 12, 20150282.

Burgess, H.J., Crowley, S.J., Gazda, C.J., Fogg, L.F., Eastman, C.I., 2003. Preflight adjustment to eastward travel: 3 days of advancing sleep with and without morning bright light. J. Biol. Rhythms 18 (4), 318–328.

Chow, E., Kessler, G., 2013. On Official Business: A Look at Secretary of State Travel. The Washington Post. 24 Jan 2013 [accessed 29 April 2017]. Available from: http://www.washingtonpost.com/wp-srv/special/politics/secretary-of-state-travel/?tid=a_inl.

Crowley, S.J., Carskadon, M.A., 2010. Modifications to weekend recovery sleep delay circadian phase in older adolescents. Chronobiol. Int. 27 (7), 1469–1492.

Czeisler, C.A., Duffy, J.F., Shanahan, T.L., Brown, E.N., Mitchell, J.F., Rimmer, D.W., et al., 1999. Stability, precision, and near-24-hour period of the human circadian pacemaker. Science 284 (5423), 2177–2181.

Dean, D.A., Fletcher, A., Hursh, S.R., Klerman, E.B., 2007. Developing mathematical models of neurobehavioral performance for the "real world". J. Biol. Rhythms 22 (3), 246–258.

Dean, D.A., Forger, D.B., Klerman, E.B., 2009. Taking the lag out of jet lag through model-based schedule design. PLOS Comput. Biol. 5 (6). E1000418.

Diekman, C., Bose, A., 2016. Entrainment maps: a new tool for understanding properties of circadian oscillator models. J. Biol. Rhythms 31 (6), 598–616.

Duffy, J.F., Wright, K.P.Jr., 2005. Entrainment of the human circadian system by light. J. Biol. Rhythms 20 (4), 326–338.

Eastman, C.I., Burgess, H.J., 2009. How to travel the world without jet lag. Sleep Med. Clin. 4 (2), 241–255.

Forger, D., Jewett, M., Kronauer, R., 1999. A simpler model of the human circadian pacemaker. J. Biol. Rhythms 14, 533–537.

Gleit, R.D., Diniz Behn, C.G., Booth, V., 2013. Modeling inter-individual differences in spontaneous internal desynchrony patterns. J. Biol. Rhythms 28 (5), 339–355.

Gonze, D., Bernard, S., Waltermann, C., Kramer, A., Herzel, H., 2005. Spontaneous synchronization of coupled circadian oscillators. Biophys. J. 89, 120–129.

Granada, A.E., Herzel, H., 2009. How to achieve fast entrainment? the timescale to synchronization. PLoS ONE 23 (4). E7057.

Guckenheimer, J., 1975. Isochrons and phaseless sets. J. Math. Biol. 1, 259–273.

Hauty, G., Adams, T., 1965. Phase Shifts of the Human Circadian System and Performance Deficit During the Periods of Transition II. West-East Flight. Federal Aviation Agency., Office of Aviation Medicine.

Hauty, G.T., Adams, T., 1965. Phase Shifts of the Human Circadian System and Performance Deficit During the Periods of Transition. I. East-West Flight. Federal Aviation Agency, Office of Aviation Medicine.

Hauty, G.T., Adams, T., 1965. Phase Shifts of the Human Circadian System and Performance Deficit During the Periods of Transition. III. North-South Flight. Federal Aviation Agency, Office of Aviation Medicine.

Herxheimer, A., Waterhouse, J., 2003. The prevention and treatment of jet lag. BMJ Brit. Med. J. 326 (7384), 296.

James, F.O., Cermakian, N., Boivin, D.B., 2007. Circadian rhythms of melatonin, cortisol, and clock gene expression during simulated night shift work. Sleep 30 (11), 1427.

Jewett, M., Kronauer, R., 1998. Refinement of a limit cycle oscillator model of the effects of light on the human circadian pacemaker. J. Theor. Biol. 192, 455–465.

Jewett, M.E., Kronauer, R.E., Czeisler, C.A., 1991. Light-induced suppression of endogenous circadian amplitude in humans. Nature 350 (6313), 59.

Johnson, C., Elliot, J., Foster, R., 2003. Entrainment of circadian programs. Chronobiol. Int. 20, 741–774.

Kelemen, M., 2016. John Kerry Heads to Antarctica and to a New travel Record. NPR Parallels. 8 Nov 2016 [accessed 29 April 2017]. Available from: http://www.npr.org/sections/parallels/2016/11/08/501153007/john-kerry-heads-to-antarctica-and-to-a-new-travel-record.

Kim, J., Forger, D., 2012. A mechanism for robust circadian timekeeping via stoichiometric balance. Mol. Syst. Biol. 8, 630.

Klein, K., Wegmann, H., 1977. Circadian performance rhythms: experimental studies in air operations. In: Mackie, R. (Ed.), Vigilance: Theory, Operational Performance and Physiological Correlates. Plenum, New York, pp. 111–131.

Kronauer, R., 1990. A quantitative model for the effects of light on the amplitude and phase of the deep circadian pacemaker., based on human data. In: Horne, J. (Ed.), Sleep '90, Proceedings of the Tenth European Congress on Sleep Research. Pontenagel Press, Dusseldorf, pp. 306–309.

Kronauer, R.E., Forger, D.B., Jewett, M.E., 1999. Quantifying human circadian pacemaker response to brief, extended, and repeated light stimuli over the photopic range. J. Biol. Rhythms 14 (6), 501–516.

Leise, T., Siegelmann, H., 2006. Dynamics of a multistage circadian system. J. Biol. Rhythms 21, 314–323.

Leloup, J., Goldbeter, A., 2013. Critical phase shifts slow down circadian clock recovery: implications for jet lag. J. Theor. Biol. 333, 47–57.

Lu, Z., Klein-Cardena, K., Lee, S., Antonsen, T.M., Girvan, M., Ott, E., 2016. Resynchronization of circadian oscillators and the east-west asymmetry of jet-lag. Chaos 26 (9), 094811.

Monk, T.H., Buysse, D.J., Carrier, J., Kupfer, D.J., 2000. Inducing jet-lag in older people: directional asymmetry. J. Sleep Res. 9 (2), 101–116.

Nakao, M., Sakai, H., Yamamoto, M., 1997. An interpretation of the internal desynchronizations based on dynamics of the two-process model. Methods Inf. Med. 36 (4–5), 282–285.

Novak, B., Tyson, J., 2008. Design principles of biochemical oscillators. Nat. Rev. Mol. Cell Biol. 9, 981–991.

Park, D.H., Kripke, D.F., Cole, R.J., 2007. More prominent reactivity in mood than activity and sleep induced by differential light exposure due to seasonal and local differences. Chronobiol. Int. 24 (5), 905–920.

Phillips, A.J., Chen, P., Robinson, P., 2010. Probing the mechanisms of chronotype using quantitative modeling. J. Biol. Rhythms 25 (3), 217–227.

Qiao, W., Wen, J.T., Julius, A., 2017. Entrainment control of phase dynamics. IEEE Trans. Automat. Control 62 (1), 445–450.

Relógio, A., Westermark, P.O., Wallach, T., Schellenberg, K., Kramer, A., Herzel, H., 2011. Tuning the mammalian circadian clock: robust synergy of two loops. PLoS Comput. Biol. 7. E1002309.

Sack, R., 2009. The pathophysiology of jet lag. Travel Med. Infect. Dis. 7, 102–110.

Sack, R.L., 2010. Clinical practice. jet lag. N. Engl. J. Med. 362 (5), 440–447.

Schmal, C., Myung, J., Herzel H. Bordyugov, G., 2015. A theoretical study on seasonality front. Neurology 6, 94.

Serkh, K., Forger, D., 2014. Optimal schedules of light exposure for rapidly correcting circadian misalignment. PLOS Comput. Biol. 10. E1003523.

Skeldon, A.C., Derks, G., Dijk, D.J., 2015. Modelling changes in sleep timing and duration across the lifespan: changes in circadian rhythmicity or sleep homeostasis? Sleep Med. Rev. 28, 96–107.

Skeldon, A.C., Dijk, D.J., Derks, G., 2014. Mathematical models for sleep-wake dynamics: comparison of the two-process model and a mutual inhibition neuronal model. PLoS ONE 9 (8). E103877.

Skeldon, A.C., Phillips, A.J., Dijk, D.J., 2017. The effects of self-selected light-dark cycles and social constraints on human sleep and circadian timing: a modeling approach. Sci. Rep. 7, 45158.

Smith, M.R., Eastman, C.I., 2012. Shift work: health, performance and safety problems, traditional countermeasures, and innovative management strategies to reduce circadian misalignment. Nat. Sci. Sleep 4, 111–132.

Song, A., Severini, T., Allada, R., 2017. How jet lag impairs major league baseball performance. Proc. Natl. Acad. Sci. USA 114 (6), 1407–1412.

Sun, M., Wang, Y., Xu, X., Yang, L., 2016. Dynamical mechanism of circadian singularity behavior in neurospora. Physica A 457, 101–108.

Takahashi, T., Sasaki, M., Itoh, H., Yamadera, W., Ozone, M., Obuchi, K., et al., 2001. Re-entrainment of the circadian rhythms of plasma melatonin in an 11-h eastward bound flight. Psychiatry Clin. Neurosci. 55 (3), 275–276.

Thorne, H.C., Jones, K.H., Peters, S.P., Archer, S.N., Dijk, D.J., 2009. Daily and seasonal variation in the spectral composition of light exposure in humans. Chronobiol. Int. 26 (5), 854–866.

Tortonese, D., Short, R., 2012. Biological rhythms, jetlag and performance in thoroughbred racehorses. Equine. Vet. J. 44 (4), 377–378.

Tortonese, D.J., Preedy, D.F., Hesketh, S.A., Webb, H.N., Wilkinson, E.S., Allen, W.R., et al., 2011. Experimental jetlag disrupts circadian clock genes but improves performance in racehorses after light-dependent rapid resetting of neuroendocrine systems and the rest–activity cycle. J. Neuroendocrinol. 23 (12), 1263–1272.

Tyson, J., Hong, C., Thron, C., Novak, B., 1999. A simple model of circadian rhythms based on dimerization and proteolysis of PER and TIM. Biophys. J. 77, 2411–2417.

Ukai, H., Kobayashi, T.J., Nagano, M., Masumoto, K.h., Sujino, M., Kondo, T., et al., 2007. Melanopsin-dependent photo-perturbation reveals desynchronization underlying the singularity of mammalian circadian clocks. Nat. Cell Biol. 9 (11), 1327–1334.

U.S. Citizen Travel to International Regions, 2017. Database: U.S. Department of Commerce, International Trade Administration. National Travel and Tourism Office. 20 October 2017 31 Jan 2017 [accessed 29 April 2017]. Available from: http://travel.trade.gov/view/m-2016-O-001/.

Van Dongen, H., 2004. Comparison of mathematical model predictions to experimental data of fatigue and performance. Aviat. Space Envir. Med. 75 (3). A15–A36.

Vosko, A.M., Colwell, C.S., Avidan, A.Y., 2010. Jet lag syndrome: circadian organization, pathophysiology, and management strategies. Nat. Sci. Sleep 2, 187–198.

Warman, V.L., Dijk, D.J., Warman, G.R., Arendt, J., Skene, D.J., 2003. Phase advancing human circadian rhythms with short wavelength light. Neurosci. Lett. 342, 37–40.

Waterhouse, J., Reilly, T., Atkinson, G., Edwards, B., 2007. Jet lag: trends and coping strategies. Lancet 369 (9567), 1117–1129.

Wever, R., 1966. The duration of re-entrainment of circadian rhythms after phase shifts of the zeitgeber a theoretical investigation. J. Theor. Biol. 13, 187–201.

Winfree, A., 1991. Circadian rhythms. resetting the human clock. Nature 350, 18.

Winfree, A.T., 1970. Integrated view of resetting a circadian clock. J. Theor. Biol. 28 (3), 327–374.

Wright, K.P.Jr., Hughes, R.J., Kronauer, R.E., Dijk, D.J., Czeisler, C.A., 2001. Intrinsic near-24-h pacemaker period determines limits of circadian entrainment to a weak synchronizer in humans. Proc. Natl. Acad. Sci. U S A 98 (24), 14027–14032.

Wright, K.P.Jr., McHill, A.W., Birks, B.R., Griffin, B.R., Rusterholz, T., Chinoy, E.D., 2013. Entrainment of the human circadian clock to the natural light-dark cycle. Curr. Biol. 23 (16), 1554–1558.

Zhang, J., Qiao, W., Wen, J.T., Julius, A., 2016. Light-based circadian rhythm control: entrainment and optimization. Automatica 68, 44–55.